JOURNAL OF AIRCRAFT
Vol. 48, No. 3, May–June 2011

Aerodynamic Considerations in the Design of Truss-Braced-Wing Aircraft

Ohad Gur,* Joseph A. Schetz,† and William H. Mason‡
Virginia Polytechnic Institute and State University, Blacksburg, Virginia 24061-0203

DOI: 10.2514/1.C031171

This paper describes a study of the effects of several key aerodynamic considerations on the conceptual design of minimum-fuel/emissions, long-range transport, transonic, truss-braced-wing aircraft configurations. This unconventional configuration has a large benefit over conventional cantilever wing configurations. The truss system enables an increased aspect ratio with lower sweep, thickness ratio, and chords, thus exploiting natural laminar flow. The design problem is solved by a multidisciplinary optimization process, which takes into account both aerodynamic and structural considerations. This paper contains several studies, each of which investigates the dependency of the design space on a specific aerodynamic parameter such as the extent of laminar flow on the wing, cruise Mach number, maximum cruise two-dimensional lift coefficient, supercritical characteristics of the airfoil, winglet influence, and intersection fairing design. In addition, various fuselage drag-reduction technologies are investigated: fuselage relaminarization, surface riblets, tailless arrangements, and Goldschmied propulsion apparatus. All of these studies illustrate the large potential of the truss-braced wing along with additional drag-reduction technologies, which may substantially decrease the fuel weight and vehicle emissions.

Nomenclature

AR	=	aspect ratio
b	=	span
C_{fairing}	=	fairing factor
$C_{\text{Goldschmied}}$	=	Goldschmied factor
C_L	=	3-D lift coefficient
C_l	=	2-D section lift coefficient
$C_{l,\max}$	=	maximum lift coefficient
c	=	chord
D	=	drag
e	=	Oswald efficiency factor
FF_{body}	=	body form factor
$FF_{\text{Goldschmied}}$	=	corrected Goldschmied form factor
FF_{wing}	=	wing form factor
H_{cr}	=	average cruise altitude
K_A	=	Korn factor
L	=	lift
L_{fuselage}	=	fuselage length
L_{laminar}	=	laminar flow length
l/d	=	fineness ratio
M	=	Mach number
M_{DD}	=	drag divergence Mach number
Re_l	=	transition Reynolds number
S_W	=	wing area
$T_{\max,\text{req}}$	=	maximum required thrust
t/c	=	section thickness ratio
W_f	=	fuel weight
W_W	=	wing weight
X, Y, Z	=	coordinates
$\Delta C_{f,\text{turbulent}}$	=	change of the turbulent skin friction
Λ_{LE}	=	leading-edge sweep angle
$\Lambda_{1/2}$	=	midchord sweep angle
$\Lambda_{1/4}$	=	quarter-chord sweep angle
$\%c_{\max,\text{laminar}}$	=	maximum laminar chordwise extent ratio

Presented as Paper 2010-4813 at the 28th AIAA Applied Aerodynamics, Chicago, IL, 28 June–1 2010; received 6 July 2010; revision received 10 October 2010; accepted for publication 21 December 2010.

*Associate Researcher, Department of Aerospace and Ocean Engineering; currently Israel Aerospace Industries, Ltd., Israel. Member AIAA.

†Professor, Frederick D. Durham Chair, Department of Aerospace and Ocean Engineering. Life Fellow AIAA.

‡Professor (Retired), Department of Aerospace and Ocean Engineering. Associate Fellow AIAA.

I. Introduction

MOST current subsonic transport aircraft bear a close resemblance to one another in their external configurations: cylindrical fuselage and cantilever wing. Such a convergence in airframe design has unfortunately resulted in a slowdown in the improvement of the aerodynamics, stability and control and structures aspects of the design, whereas impressive advancements have been reported in the development and integration of aeronautical avionics, propulsion systems, and subsystems. Industry and NASA have sought changes in the configuration of conventional takeoff and landing aircraft that could make major increases in performance [1]. One approach is to pursue substantial increases in the lift-to-drag ratio L/D with a recent goal stated to be double that of existing configurations. This would result in major reductions in fuel consumption, emissions, and noise. Another approach is to directly pursue significant reductions in fuel consumption and the corresponding emissions. Truss-braced-wing (TBW) configurations are one attractive path to considerably enhancing the aerodynamic efficiency of a conventional takeoff and landing aircraft [2].

Some of the technological advances that will enable achievement of the aggressive goal of large improvements in aircraft performance can be summarized as 1) truss-braced wings, 2) natural laminar flow, 3) fuselage modifications to reduce wetted area, 4) engines buried in the fuselage and Goldschmied apparatus [3], 5) thrust vectoring, and 6) wing-tip-mounted engines or other wing-tip treatments. Modifications in the flight path and the use of biofuels are also attractive possibilities.

An early suggestion for a truss-braced-wing arrangement for a large transonic transport aircraft is shown in Fig. 1. Following Pfenninger's footsteps [4], the concept of a strut-braced-wing (SBW) configuration was investigated using multidisciplinary design optimization (MDO) tools [5–7]. These studies established the potential benefits of such configurations. Truss-braced wings can be thin and with reduced sweep, which are both important for achieving significant areas of natural laminar flow as well as reducing manufacturing costs. Of course, the issue of interference drag penalties needs careful study [8]. This configuration also has the potential to reduce wing weight by as much as 70%. Large decreases in induced

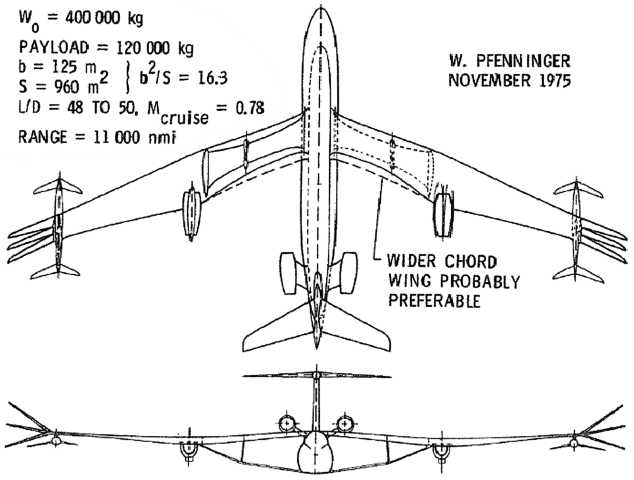

Fig. 1 One of Pfenninger's visions [4] for a truss-braced-wing aircraft.

drag can be attained by increasing the wingspan. The use of trusses and folding wing extensions make this possible. Induced drag reductions of about 75% have been projected. The attendant reductions in wing chord imply more drag reduction from natural laminar flow.

Successful implementation of this concept will clearly require careful structural analysis and design. Stiffness and aeroelastic considerations will play an important role in the design. The key problem will be to optimize the locations and appropriate stiffness of each of the truss members. An MDO framework that was developed especially for this purpose is used in the current research [9]. This paper contains a brief description of this framework and its main design modules.

Green [10] reviewed some of the aerodynamic aspects while focusing on friction-drag reduction using laminar flow control. Structural aspects for a conventional cantilever wing limit the potential reduction of thickness-to-chord ratio or an increase in wingspan, due to the large weight penalty, thereby limiting performance improvements for a conventional cantilever wing configuration.

Changes in the current fuselage configuration can lead to significant reductions in viscous drag. The basic notion is to reduce wetted area. The use of riblets and other surface features also lead to reduced viscous drag. One should also consider mounting the engines in the fuselage base along with boundary-layer inlets and Goldschmied shrouds. This is estimated to produce about a 20% increase in propulsive efficiency. Thrust vectoring can be employed for control, possibly eliminating the empennage, provided vehicle airworthiness can be guaranteed through a fault-tolerant design.

This paper will focus on aerodynamic considerations in the design of truss-braced-wing aircraft. The main topics covered will include effects of the various aerodynamic parameters, each of which refers to different aerodynamic technologies: natural laminar flow (NLF), maximum 2-D lift coefficient, airfoil design, cruise Mach number, winglets, interference drag and fairing; fuselage treatments including riblets, relaminarization, Goldschmied apparatus, and tailless configurations. These studies shed light on the potential of the aerodynamic design of the truss-braced wing and in some cases for other configurations. In addition, comparing the various studies reveals the relative importance of each technology, and thus giving some idea into which of these technologies is worthwhile to be further developed.

II. TBW Problem Statement

The main TBW design requirement considered here is the accomplishment of a mission that is defined here as flying a range of 7730 NM with 305 passengers (see Fig. 2), which is very similar to that of the Boeing 777-200ER. The aircraft is a high-wing configuration, integrated with truss structures, T-tail, with fuselage based on the Boeing 777–200ER, and it is powered by two high-bypass-ratio turbofan fuselage-mounted engines.

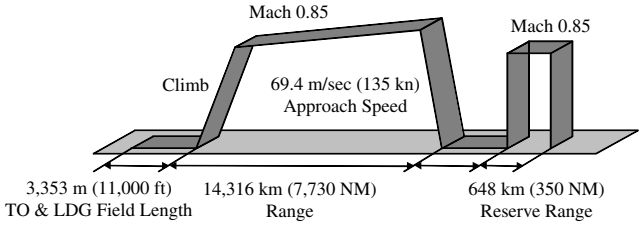

Fig. 2 Basic mission used for our design.

Various goals can be considered when designing an air vehicle [11,12], with an appropriate definition of the objective function for each goal. Possible goals may be minimum takeoff gross weight (TOGW), minimum fuel/emissions, and maximum lift-to-drag ratio. These three figures of merit represent different emphases. The minimum-fuel objective function emphasizes lower operational cost and lower emissions and is used in the current MDO study.

Design constraints are imposed on performance, such as takeoff and landing field length, minimum rate of climb after takeoff, single engine flight, etc. Additional constraints are imposed on maximum wing deflection while encountering a taxi bump and sufficient fuel capacity as dictated by the mission.

The design variables include geometric parameters for both the wing and the truss system: wingspan; wing thickness-to-chord ratios, chords, and sweep; and strut/truss-member length. In addition, two operational variables are used as design variables: required thrust and cruise altitude.

III. Design Environment Description

A detailed description of the design environment and its various analysis modules is presented in [9], and a schematic of the framework components is shown in Fig. 3. The main analyses (propulsion, aerodynamics, structures, and weight estimation) are located in the weight convergence loop, while the calculation of the design goals and constraints is done as part of the outer optimization loop.

For a given set of design variables (configuration) and flight conditions, the TOGW is found iteratively. Note that the cost function that is used here is the fuel weight and not TOGW. This is done mainly due to the varying engine size, which influences the vehicle TOGW and drag, and also due to the c.g. location, which influences the trim drag. The outer optimizer loop includes the

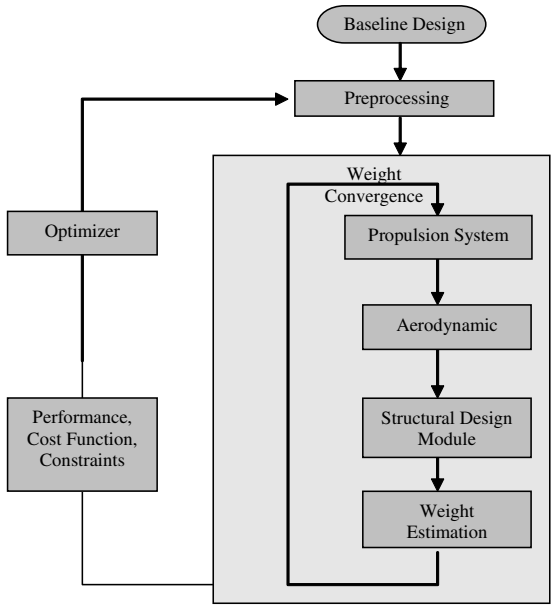

Fig. 3 TBW design framework schematic.

Fig. 4 Wing and truss-member cross sections are idealized to be made up of upper and lower equivalent skins.

different optimizer modules such as the Vanderplaats Research & Development Design Optimization Tools [13], Design Explorer [14], etc. In the current research, the DOT optimizer with a modified feasible direction scheme is used.

The following sections present short descriptions of the structural design module and the aerodynamic analysis module, which are the main components of the design environment.

A. Structural Design Module

The structural design module calculates the structural weight and deflections of the wing under various loading conditions. For a given wing/truss geometric configuration, aerodynamic load, and fuel loading distribution, the structural module is used to calculate the minimum amount of material required such that the maximum stress in all structural members is below the specified material limit, and that none of the truss members buckle under a negative 1-*g*-load case [9].

The structural module is based on a combination of finite element analysis of the wing/truss configuration and the fully stressed design criteria. The structure is modeled with beam finite elements that have four stiffness components related to transverse and chordwise bending displacements, axial displacement, and torsional rotation. The stiffness is calculated using an equivalent beam model of the wing box, as shown in Fig. 4. The upper-skin thickness is assumed to be equal to the lower-skin thickness, and the leading-edge spar web is assumed to have the same skin thickness as the trailing-edge spar web.

The material properties assumed for the current study are given in Table 1. Note that the use of composite materials is outside the scope of this study. A safety factor of 1.5 is used for each load case, and the total loading is a combination of the aerodynamic lift, fuel inertia loads and self-weight inertia of the structural elements.

A total of 19 load cases are considered for structural sizing:

1) A $+2.5$ *g* pull-up maneuver occurs at 0, 50, and 100% fuel.

2) A -1.0 *g* maneuver occurs at 0, 50, and 100% fuel.

3) A 2 *g* taxi bump occurs at 100% fuel (does not include aerodynamic lift).

4) Six gust-load cases occur with 0% fuel, and Federal Aviation Regulations (FAR) discrete vertical gusts are specified at different altitudes: 0 ft, 3048 m (10,000 ft), 6096 m (20,000 ft), 9144 m (30,000 ft), and 12,192 m (40,000 ft).

5) Six gust-load cases occur with 100% fuel, and FAR discrete vertical gusts are specified at different altitudes: 0 ft, 3048 m (10,000 ft), 6096 m (20,000 ft), 9144 m (30,000 ft), and 12,192 m (40,000 ft).

Although these load cases do not cover the entire FAR requirements, they represent most of the flight envelope.

The different flight conditions that are used as structural load cases are defined by the flight altitude, Mach number, lift coefficient, configuration (fuel and cargo percentage), and inertial load factor.

Table 1 Aluminum material (Al-7075 [15]) properties assumed for current study

Material property	Value
Young's modulus	71.8×10^9 Pa (1.5×10^9 psf)
Poisson ratio	0.33
Density	2883 kg/m^3 (180 lb/ft^3)
Max allowable stress	383×10^9 Pa (8×10^6 psf)

The gust loading is derived from a simple one-degree-of-freedom representation [16].

The gate-box limit of 80 m (262.5 ft)[§] is addressed by assuming that a folding mechanism can be designed to fold the wings and reduce the parking width of the aircraft. The folding joint is assumed to be at 40 m (131 ft) on the wing, and a weight penalty is added as a dead mass at the joint location, following the Boeing design for a folding-tip option on the 777 [17]. Detailed description of this weight penalty model is available in [9]. Note that except for the 80 m gate-box limit, no other wingspan limit is considered.

Note that the fully stressed design approach dictates that each element be sized so that it carries the maximum allowable stress. Hence, this approach cannot be used to satisfy a displacement constraint if the design process involves only structural sizing. The displacement constraint is handled by the outer MDO process.

The module calculates the load bearing mass of the wing. The other components of the wing mass (spar and rib webs and secondary structure) are added using FLOPS (Flight Optimization System), developed by NASA [18].

B. Aerodynamic Analysis Module

The aerodynamic module calculates the drag and structural loading for a given configuration. The drag bookkeeping is based on semi-empirical methods presented in [19].

The optimum wing loading for a given geometry is calculated using a Trefftz Plane analysis [20,21]. In addition to the optimal spanwise lift distribution, this analysis computes the minimum induced drag. Each flight condition (representing a different load case or performance constraint) is defined using the Mach number, flight altitude, and lift coefficient. For this set of parameters, the optimized wing loading is calculated and used as input for the structural module or for the performance calculation through the induced drag.

The induced drag, combined with the friction, wave, and interference drag components define the total drag of the vehicle configuration. This drag breakdown is presented in Fig. 5 and thoroughly described in [19].

The friction-drag calculation is based on the wetted area and uses predictions from skin-friction models and form-factor estimations. The skin-friction prediction uses laminar and turbulent boundary-layer models. For laminar flow, the Eckert reference-temperature method [22] is used, and for turbulent flow the Van Driest II method [23,24] (based on the von Kármán–Schoenherr model) is used. The total skin-friction coefficient is based on a composite of the laminar/turbulent flow. For the current research, Schlichting's composite formula is used [25]. The complete model for the flat-plate skin-friction coefficient is available online.[¶]

Different transition criteria are considered through a technology factor (TF) parameter, where $0 < \mathrm{TF} < 1$. This simple approach is used to determine the chordwise location of boundary-layer transition dependencies on sweep and Reynolds number. Figure 6 presents two curves of transition Reynolds number based on the chordwise Reynolds number Re_l, taken from [26]. The dashed curve designated as $\mathrm{TF} = 0$ (technology factor of 0) is for natural laminar flow on standard wings [27]. The solid curve, designated as $\mathrm{TF} = 1$, refers to natural-laminar-flow airfoils [28].

The flat-plate equivalent transition Reynolds number on the fuselage can also be estimated. In addition, riblets can be used, and thus the turbulent friction coefficient for the fuselage can be decreased between 3 and 7% [29].

A form factor is used to represent the drag correction due to both thickness and pressure drag, which is sometimes referred to as profile drag. Many form-factor models exist [30–35]; the current research uses the Grumman lifting-surface form factor for the wing, truss members, and tail (FF_{wing}):

[§]This is the FAA category VI (or ICAO category F) limit that is currently applicable for the Airbus 380.

[¶]Data available online at http://www.aoe.vt.edu/~mason/Mason_f/FRICTman.pdf [retrieved 1 July 2010].

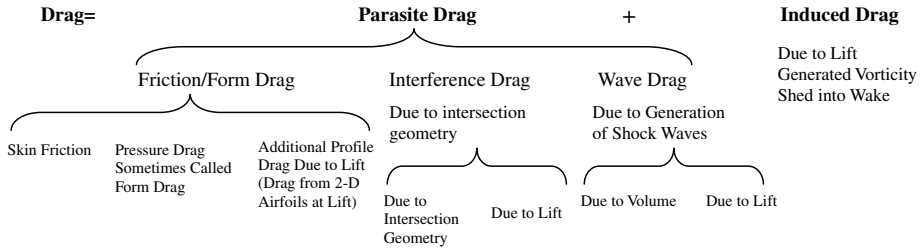

Fig. 5 Drag breakdown.

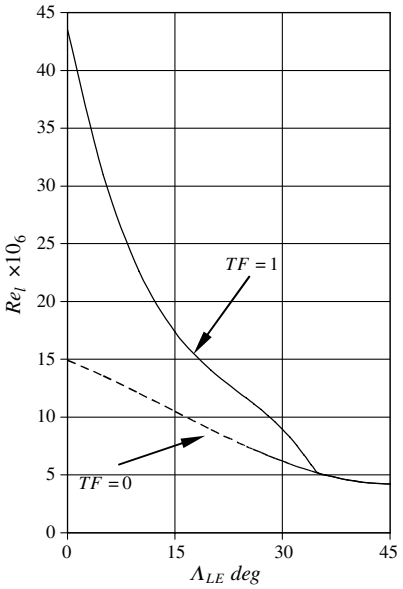

Fig. 6 Wing transition Reynolds number and TF definition [26].

$$FF_{\text{wing}} = 1 + 1.8\frac{t}{c} + 50\left(\frac{t}{c}\right)^4 \tag{1}$$

where t/c is the maximum thickness ratio of the cross section.

The Hoerner [30] body-of-revolution form factor, FF_{body}, was used for the fuselage and nacelles:

$$FF_{\text{body}} = 1 + \frac{1.5}{(l/d)^{1.5}} + \frac{7}{(l/d)^3} \tag{2}$$

where l/d is the body fineness ratio.

The wave-drag model used in this study is based on the Korn equation extended to swept wings , where a Korn factor of 0.95 implies the use of advanced supercritical airfoils, and a Korn factor of 0.87 represents the use of a conventional airfoil. Along with Lock's fourth power law [37–39], the drag rise, critical Mach number, and drag-divergence Mach number M_{DD} can be estimated.

Interference drag results from the airflow over the intersection of a lifting or truss-member surface with either the fuselage or with another lifting surface. The fuselage/wing and truss/wing interference drag are modeled using methods given by Hoerner [30] and precomputed drag response-surface models obtained from viscous computational fluid dynamics simulations [40]. The truss/strut intersections share similar chord lengths; thus, the interference drag is based on drag response surfaces obtained from viscous computational fluid dynamics simulations of two similar-chord wing intersections [8].

Note that these interference drag models do not include any fairing effects. According to the literature, a fairing is able to reduce the interference drag by at least by 90% (a factor of 0.1) [30] and in certain cases even to make the interference drag negligible [33,35,41]. This suggests that a conventional fairing factor is about 0.1, and aggressive fairing is represented by factor of 0.02.

Table 2 Design constraints

Constraint	Value
Range	≥14,316 km (7730 n mile) with additional 648 km (350 n mile) for reserve
Initial cruise rate of climb	≥ 1.524 m/s (300 ft/ min)
Maximum section C_l in cruise	≤ 0.8
Available fuel volume	≥ required fuel
Wing deflection	≤ 6.19 m (20.3 ft)
Second-segment climb gradient	≥ 2.4%
Approach velocity	≥ 68.16 m/s (132.5 KTAS)
Missed approach climb gradient	≥ 2.1%
Balanced field length	≤ 3353 m (11,000 ft)

IV. Baseline Design

The baseline design was a two-jury TBW presented previously in [9]. Four different configurations were designed: cantilever, SBW, single-jury TBW, and two-jury TBW. The cost function was minimum-fuel weight/emissions, and the design constraints are summarized in Table 2 and detailed in [2]. Most of the constraints relate to performance and some to other considerations such as available fuel volume and wing deflection constraints.

The design variables are the wing and truss-system sizing variables. These include the definition of the wing-section midchord coordinates, chords, and thickness ratios. Figure 7 presents the section locations for the two-jury TBW configuration, and Table 3 contains the design variables used for this configuration. Note that the truss members have both a constant chord and constant thickness-to-chord ratio, and the wing has a constant quarter-chord sweep. This reduces the number of design variable [9], since some of the cross section's properties are prescribed using interpolation of other cross sections. Similar design variables and considerations are also used for the single-jury TBW, SBW, and the cantilever configuration.

Two additional design variables appear in Table 3: thrust and fuel weight. The thrust is the engine sizing variable, and the fuel weight is found based on to the required range constraint.

The cruise is flown at an average cruise altitude of $H_{\text{cr}} = 14,630$ m (48,000 ft) and constant Mach number $M = 0.85$. Previously, the average cruise altitude was one of the design variables, with a side constraint of $H_{\text{cr}} < 14,630$ m (48,000 ft). All of the resulting minimum-fuel/emissions designs reached this side constraint; thus, it was decided to prescribe the altitude and remove it from the design variables. A weight penalty model is used to account for the fuselage pressurization weight due to this increased altitude [31]. Note that the Concorde was cruising at 56,000 ft; thus, an altitude of 48,000 is not considered to be extremely high.

The baseline configurations were designed considering an aggressive NLF; thus, the laminar technology factor is set to TF = 1 (see Fig. 6). The chordwise length of the laminar flow is limited to 70% of the local chord. The airfoil is considered to be a supercritical one (Korn factor of 0.95), and the maximum 2-D cruise lift

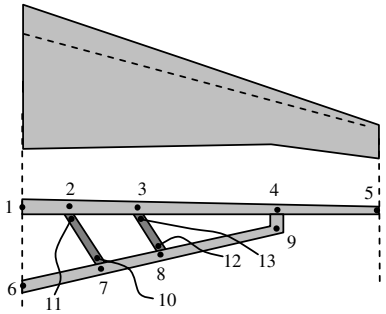

Fig. 7 Definition of two-jury TBW cross sections.

coefficient is set to $C_{l,\max} = 0.8$. These considerations represent a very advanced airfoil and wing design, as expected from an $N + 3$ (2030) design.** The fairing factor is set to 0.02, representing an advance fairing design that minimized the interference drag penalties.

As stated above, the fuselage is similar to the 777-200ER, 62.8 m (206 ft) length, but with fuselage-mounted engines and a T-tail. The transition Reynolds of the fuselage is assumed to be $Re_l = 2.5 \times 10^6$. At the specified cruise conditions, the value of 2.5×10^6 (which might represent an *aggressive laminar* condition) is equivalent to about 0.7 m (2.2 ft), which for the 62.8 m (206 ft) fuselage means practically a fully turbulent fuselage, $L_{\text{laminar}}/L_{\text{fuselage}} = 0.01$. L_{laminar} and L_{fuselage} are the lengths of the laminar flow and the fuselage, respectively. In addition, the fuselage and engine nacelles are considered to be covered with riblets that decrease the turbulent friction drag by $\Delta C_{f,\text{turbulent}}$ of 5%.

Figure 8 presents the optimized configuration for the minimum-fuel design cases for the cantilever (Fig. 8a), strut-braced wing (Fig. 8b), jury truss-braced wing (Fig. 8c), and two-jury truss-braced wing (Fig. 8d). The most noticeable feature is the change of planform with increased complexity of the wing topology. As additional truss members increase the wingspan and decrease the chords, the wing aspect ratio is increased. In addition, the chord of the main strut is decreased as truss members are added, and the strut-wing intersection is pushed toward the wing tip.

These trends are shown in Fig. 9, which presents the change of the following parameters for the four different configurations: fuel weight (the design cost function) W_f, TOGW, wing weight W_W, wing area S_W, quarter-chord sweep angle $\Lambda_{0.25}$, half-span $b/2$, lift-to-drag ratio L/D, aspect ratio AR, and wing loading TOGW/S_W.

Of the four configurations, the two-jury TBW exhibits the lowest fuel weight; thus, it is used for the trend studies that are presented in the following sections.

V. Aerodynamic Trend Study

As stated above, the baseline configuration for the following aerodynamic study is the two-jury TBW optimized for minimum fuel/emissions, as presented in Fig. 8d. To explore the aerodynamic considerations that influence the optimized design, a sensitivity study was performed for the various aerodynamic parameters. For each study, one parameter is altered and the others are kept the same as in the baseline configuration (Fig. 8d). Then a new optimized set of the design variables (Table 3) is found by the MDO process. This is repeated for different values of the relevant parameter; thus, the dependency of the design with that parameter is investigated.

Table 4 summarizes the following parameters, which are used in this study, and they are described below.

1) *Laminar technology factor TF*: As shown in Fig. 6 the range of the laminar TF is 0 (conventional wing) to 1 (aggressive laminar wing). The baseline configuration uses the aggressive laminar, TF = 1, which is based on the F-14 glove experiment [42]. The study

Table 3 Two-jury TBW design variables

No.	Variable	Nomenclature
1	Cross section 1: chord	c_1
2	Cross section 1: thickness ratio	t/c_1
3	Cross section 2: Y coordinate	Y_2.
4	Cross section 3: Y coordinate	Y_3
5	Cross section 4: Y coordinate	Y_4
6	Cross section 4: chord	c_4
7	Cross section 4: thickness ratio	t/c_4
8	Cross section 5: X coordinate	X_5
9	Cross section 5: Y coordinate	Y_5
10	Cross section 5: chord	c_5
11	Cross section 5: thickness ratio	t/c_5
12	Cross section 6: X coordinate	X_6
13	Cross section 6: chord	c_6
14	Cross section 6 thickness ratio	t/c_6
15	Cross section 7: Y coordinate	Y_7
16	Cross section 8: Y coordinate	Y_8
17	Cross section 9: Z coordinate	Z_9
18	Cross section 10: chord	C_{10}
19	Cross section 10 thickness ratio	t/c_{10}
20	Cross section 12: chord	C_{12}
21	Cross section 12: thickness ratio	t/c_{12}
22	Average cruise altitude	H_{cr}
23	Takeoff fuel weight	W_f
24	Maximum required thrust	$T_{\text{max,req}}$

was done for the range $0 < \text{TF} < 1.2$, where TF = 1.2 represents a futuristic wing design that has a higher transition Reynolds than the one stated in Fig. 6 for TF = 1. Such a curve was suggested by Green [10].

2) *Quarter-chord sweep angle* $\Lambda_{1/4}$: The baseline design main wing has a quarter-chord sweep angle of $\Lambda_{1/4} = 27.2$ deg. To explore the reason for such high sweep although using TF = 1, fixed quarter-chord sweep configurations were designed using $\Lambda_{1/4} = 20$ and 15 deg.

3) *Maximum chordwise laminar extent ratio* $\%c_{\text{max,laminar}}$: The baseline lifting surfaces are limited to 70% chordwise laminar flow ($\%c_{\text{max,laminar}}$). Note that this limitation is implied for both the upper and lower part of the lifting surfaces (wing, truss members, tail). The study used a range of 40 to 100% chordwise laminar flow limit. The baseline configuration also uses TF = 1; thus, the wing has aggressive NLF characteristics, which emphasizes the importance of the chordwise laminar ratio limitation.

4) *Maximum 2-D cruise lift coefficient* $C_{l,\max}$: The 2-D sectional lift coefficient at cruise is limited to $C_{l,\max} = 0.8$ for the baseline design. To explore the influence of this parameter, a range of 0.6 to 1.0 was investigated.

5) *Korn factor* K_A: A Korn factor of $K_A = 0.87$ represents a conventional airfoil, and $K_A = 0.95$ stands for supercritical airfoil. The baseline design uses 0.95; thus, the influence of a less advanced supercritical design was investigated.

6) *Cruise Mach number* M: The common assumption is that flying at a lower Mach number might improve the vehicle efficiency. While the baseline vehicle is considered to fly at $M = 0.85$, the impact of lower Mach numbers in the 0.7–0.85 range was investigated. The study is conducted twice, once with a fixed cruise altitude and then using the cruise altitude as a design variable.

7) *Wing-tip-treatment influence*: The baseline configuration has a planar main wing with an additional truss system. To find the influence of a nonplanar wing, the influence of a simple winglet tip was investigated.

8) *Fairing factor* C_{fairing}: The interference drag was studied with a fairing factor C_{fairing} that ranges from 0.02 (baseline configuration) to 0.2. This illustrates the effect of very careful or minimal fairing of the wing and truss-member intersection.

9) *Fuselage relaminarization, or fuselage laminar flow ratio* $L_{\text{laminar}}/L_{\text{fuselage}}$: A way of decreasing the fuselage drag is through relaminarization of the fuselage boundary layer. This is proposed to be done after the cockpit area and entrance door through

**NASA study looking at advanced concepts and technologies for aircraft in the 2030–2035 time frame.

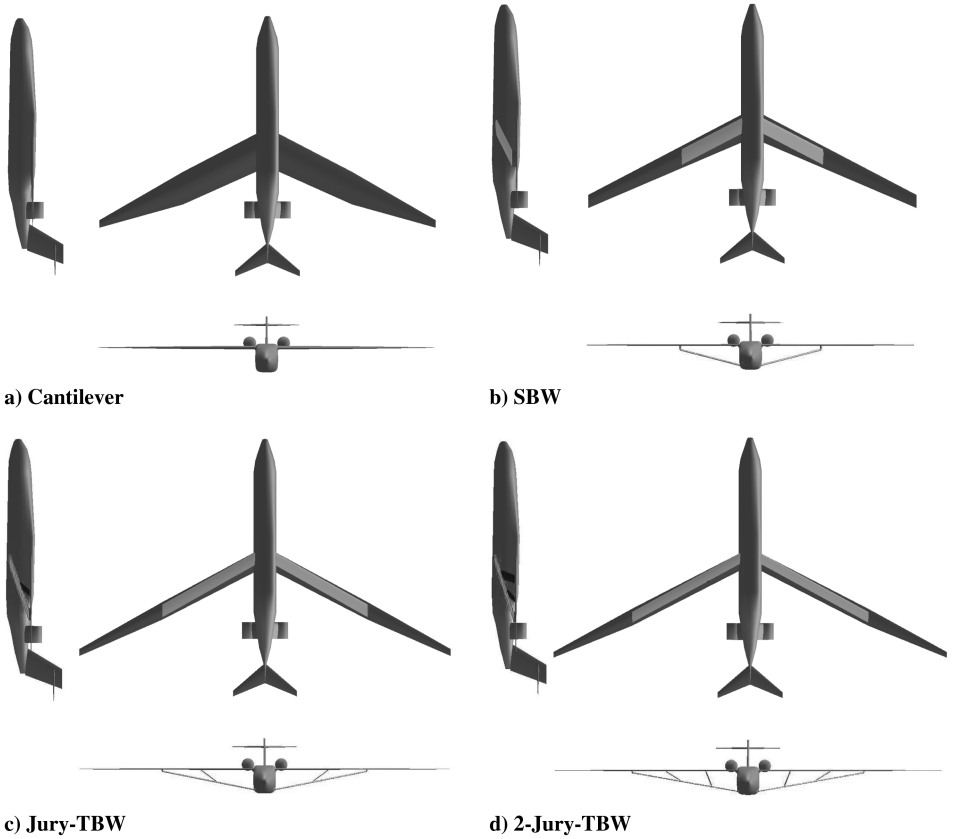

a) Cantilever b) SBW

c) Jury-TBW d) 2-Jury-TBW

Fig. 8 Baseline optimized minimum-fuel configurations.

boundary-layer suction. To model this option, the transition Reynolds number for the fuselage was increased up to a value of 169.3×10^6, which is equivalent (at cruise flight conditions) to $L_{\text{laminar}}/L_{\text{fuselage}} = 0.75$ (0.75 of the fuselage length experiences laminar flow). The weight penalty due to the relaminarization devices has not been modeled.

10) *Riblet turbulent skin-friction reduction* $\Delta C_{f,\text{turbulent}}$: The use of riblets decreases the turbulent skin friction. The baseline uses a $\Delta C_{f,\text{turbulent}}$ of 5%, and values of 0 and 7% were studied.

11) *Goldschmied fuselage factor* $C_{\text{Goldschmied}}$: A possible potential for fuselage drag reduction is the Goldschmied apparatus [3]. Goldschmied proposed sucking off the turbulent boundary layer through a slot toward the rear of the fuselage and using that fluid in a submerged engine (see Fig. 10). This is claimed to produce increased static pressure on the rear of the fuselage resulting in thrust. Although this apparatus was presented by Goldschmied [3] as a means of "self-propulsion by static-pressure thrust," he also admitted that: ". . .any device which can manipulate the boundary layer...would be able to eliminate the form drag..." and in a different place: "what body thrust force occurs to offset most of the turbulent friction drag." Thus, aerodynamic representation of the Goldschmied apparatus is introduced here as an updated form factor, $FF_{\text{Goldschmied}}$:

$$FF_{\text{Goldschmied}} = FF_{\text{body}} - C_{\text{Goldschmied}} \tag{3}$$

where FF_{body} is the original body form factor and $C_{\text{Goldschmied}}$ is the Goldschmied factor, which ranges from 0 (for a conventional fuselage) to 1 (for total elimination of the friction drag). The authors are aware that the Goldschmied apparatus will include some weight penalty. But for the current trend study, no model of that effect was included.

12) To explore a possible use of thrust vectoring, a tailless configuration was designed. This configuration exploits aerodynamic trim; thus, the thrust penalty of the propulsion system is neglected. To explore the influence of using thrust vectoring along with a Goldschmied apparatus, a combined configuration was designed.

A. Laminar TF Influence

Figure 11 shows the optimized configurations for three different technology factors, TF = 0.0, 1.0 (baseline), and 1.2. Figure 12 presents the dependency of the following parameters with the TF: fuel weight W_f, aspect ratio AR, lift-to-drag ratio L/D, quarter-chord sweep $\Lambda_{0.25}$, TOGW, wing weight W_W, half-span $b/2$, wing area S_W, and wing loading TOGW/S_W.

Table 4 Sensitivity-study parameters

Parameter	Nomenclature	Min. value	Max. value	Baseline value
Laminar technology factor	TF	0.0	1.2	1.0
Quarter-chord sweep angle, deg	$\Lambda_{1/4}$	15	27.2	27.2
Maximum chordwise laminar extent ratio	$\%c_{\text{laminar}}$	40%	100%	70%
Maximum 2-D section lift coefficient	$C_{l,\max}$	0.6	1.0	0.8
Korn factor	K_A	0.87	0.95	0.95
Cruise Mach number	M	0.7	0.85	0.85
Fairing factor	C_{fairing}	0.02	0.2	0.02
Fuselage laminar flow ratio	$L_{\text{laminar}}/L_{\text{fuselage}}$	0.01	0.75	0.01
Riblet turbulent skin-friction reduction	$\Delta C_{f,\text{turbulent}}$	0%	7%	5%
Goldschmied factor	$C_{\text{Goldschmied}}$	0.0	1.0	0.0

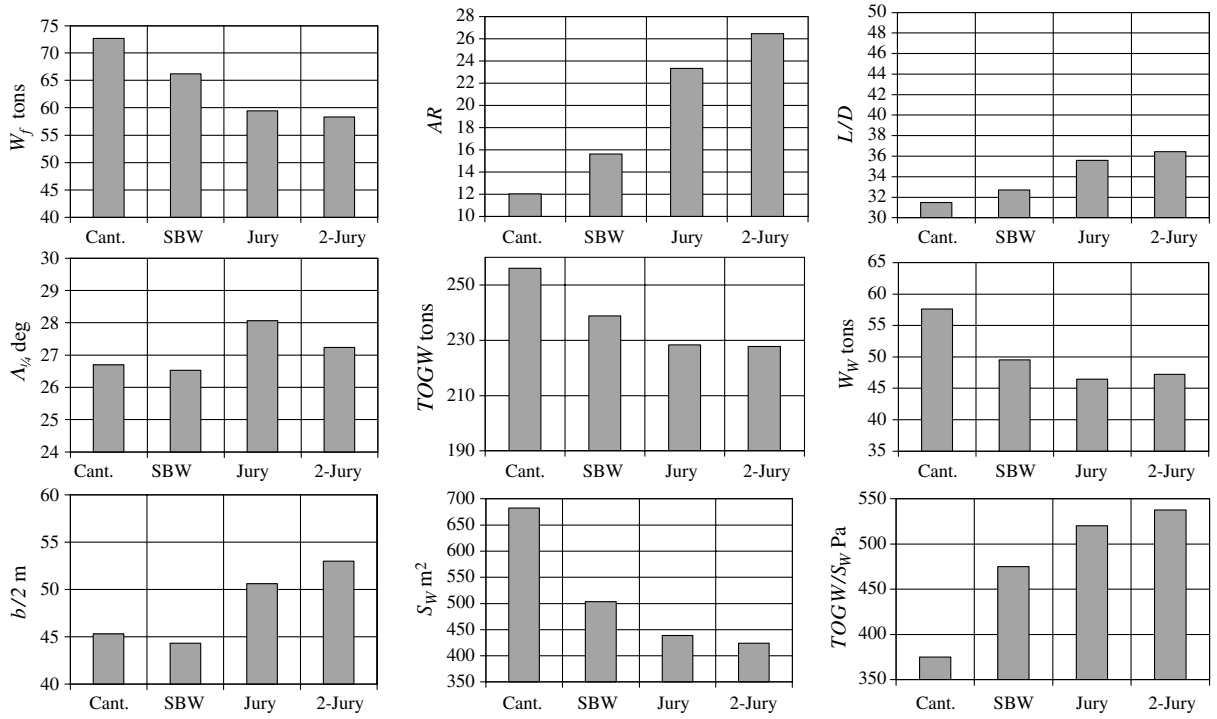

Fig. 9 Baseline optimized minimum-fuel configurations, parametric study.

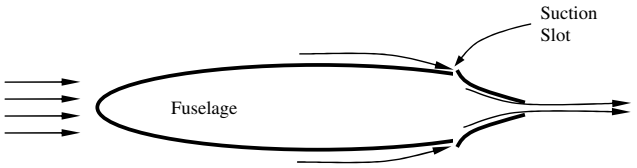

Fig. 10 Schematic of Goldschmied apparatus.

The active constraints for all of the configurations are the range and the maximum 2-D lift coefficient. Note that the 2-D maximum cruise lift coefficient constraint is the one that limits the wing chord from becoming too small, while higher aspect ratio (decreased chords) increases the vehicle efficiency.

As the technology factor is increased, the fuel weight is decreased due to the increased laminar flow. This is accompanied with increased lift-to-drag ratio and increased aspect ratio.

Comparing the vehicle planforms shows a small difference. As the technology factor is increased, the wing sweep is decreased from 28 deg (TF = 0) to 27 deg (TF = 1.2). This minor reduction shows that although lower sweep contributes to NLF (as shown in Fig. 6), the sweep angle has to remain relatively high. This is further explained in Fig. 13, which shows the configuration drag breakdowns. Although the friction drag of the wing is decreased as TF increases, the wave drag is increased due to the lower sweep angle. This places the increased wave drag as a counterbalance to the decreased friction drag.

Figure 14 presents the dependency of the wave and friction drag with varying quarter-chord sweep angle of the baseline configuration. These results were obtained by changing the main wing sweep of the baseline design. The baseline configuration represents the sweep angle where the rate of change of the friction drag starts to increase and the rate of change of the wave drag starts to decrease. Thus, at a sweep angle of 27 deg the gradient of the friction and wave drag share similar values with opposite signs.

Recall that the chordwise transition location is limited to 0.70 ($\%c_{\max,\text{laminar}} = 70$). Figure 15 shows the main wing chordwise transition ratio. It is clear that the chordwise transition ratio limitation is an important parameter, which together with TF establishes the laminar flow properties of the wing. This is true mainly for the outer part of the wing, which has a smaller chord; thus, the chordwise transition limitation is reached even for low TF.

B. Quarter-Chord Sweep Angle

As stated in the previous section, the influence of the NLF on the wing sweep angle is small. To investigate it, two fixed-sweep configurations were designed with $\Lambda_{1/4} = 20$ and 15 deg. Figure 16 shows the optimized configurations. Figure 17 presents the dependency of the design parameters on the quarter-chord sweep. The active constraint for the $\Lambda_{1/4} = 20$ deg is still the range and the maximum 2-D lift coefficient, but for the $\Lambda_{1/4} = 15$ deg the fuel volume constraint is active. This is due to the increased required fuel volume for the lower-sweep-angle configuration.

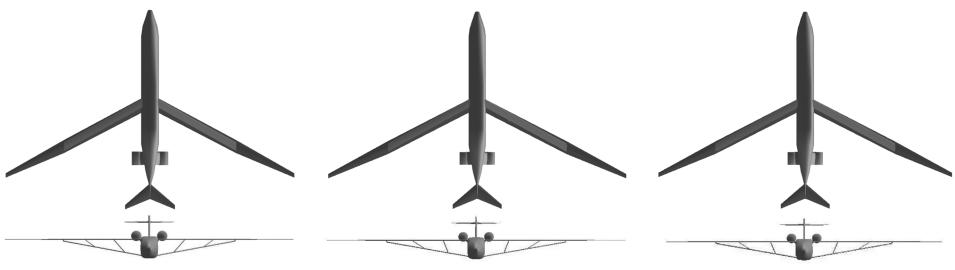

a) TF = 0.0 **b) TF = 1.0 (baseline)** **c) TF = 1.2**

Fig. 11 Laminar TF study, configurations.

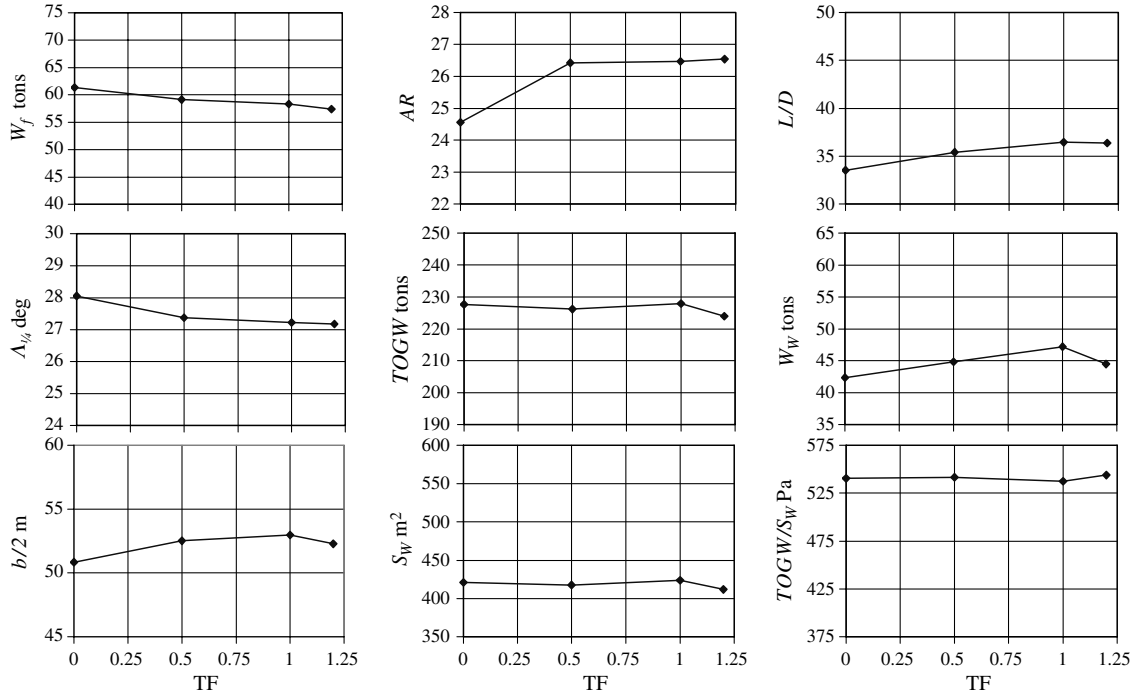

Fig. 12 Laminar TF study, key parameters.

As the quarter-chord sweep is decreased, the L/D is decreased because the wave drag goes up sharply and the friction drag hardly changes (see Fig. 18). The gain in NLF at lower sweep angles is only to maintain laminar flow up to the 70% limit over the whole wing, compared with 60% in the inboard region of the wing for the baseline design (see Fig. 19). Note that the truss does its job, not only leading to lower chords and thus lower chord Reynolds numbers to help with NLF, but also leading to low-t/c wings and truss members. This helps to minimize wave drag.

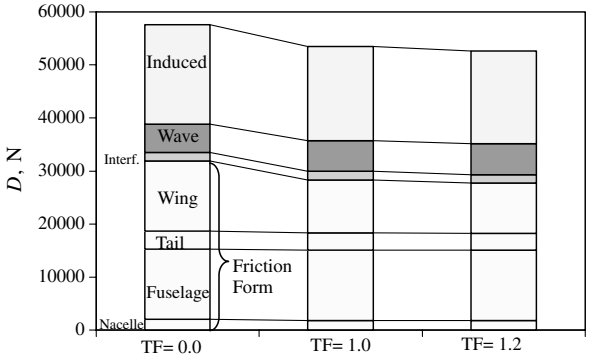

Fig. 13 Laminar TF study, drag breakdown.

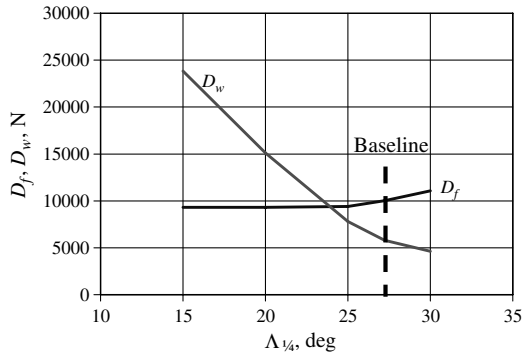

Fig. 14 Dependency of the friction and wave drag with quarter-chord sweep angle.

C. Maximum Chordwise Laminar Extent Ratio Influence

To investigate the influence of the chordwise laminar extent ratio limit, several configurations were designed with different values of the maximum chordwise laminar ratios, $\%c_{\text{max,laminar}}$. Figure 20 shows the optimized configurations for three different chordwise laminar length limits: $\%c_{\text{max,laminar}} = 40$, 70 (baseline), and 100. Figure 21 presents dependency of the design parameters on the chordwise laminar length limits. The active constraint is still the range and the maximum 2-D lift coefficient for all of the configurations.

The maximum chordwise laminar extent ratio has a distinct impact on the vehicle geometry. As the chordwise length of laminar flow is increased, the wing chord is reduced, aspect ratio is increased and the lift-to-drag ratio is increased. All of these trends result in a decreased fuel weight.

As in the TF study, the wing sweep is decreased slightly as $\%c_{\text{max,laminar}}$ is increased. This results in decreased friction drag (due to higher transition Reynolds number) and increased wave drag (Fig. 22). The chordwise laminar extent ratios of the main wing are presented in Fig. 23. As in the TF study (Fig. 15), it emphasizes the close relation of TF and $\%c_{\text{max,laminar}}$. The use of high TF with low $\%c_{\text{max,laminar}}$ does not enable full exploitation of NLF potential. Still, even when a full exploitation of the NLF occurs, ($\%c_{\text{max,laminar}} = 100$) the sweep angle does not decrease significantly.

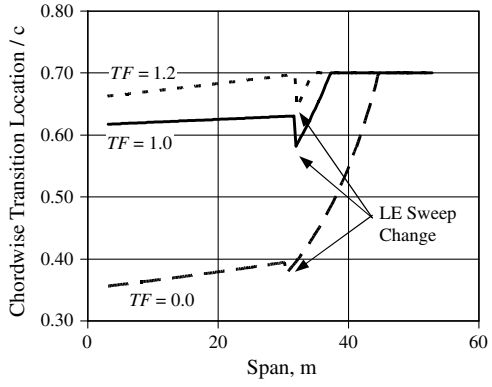

Fig. 15 Laminar TF study, main wing chordwise transition location.

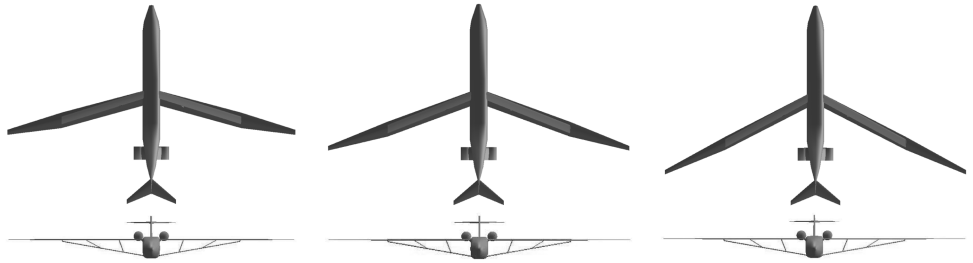

a) $\Lambda_{1/4}$ = 15 deg b) $\Lambda_{1/4}$ = 20 deg c) $\Lambda_{1/4}$ = 27.2 deg

Fig. 16 Quarter-chord sweep-angle study, configurations.

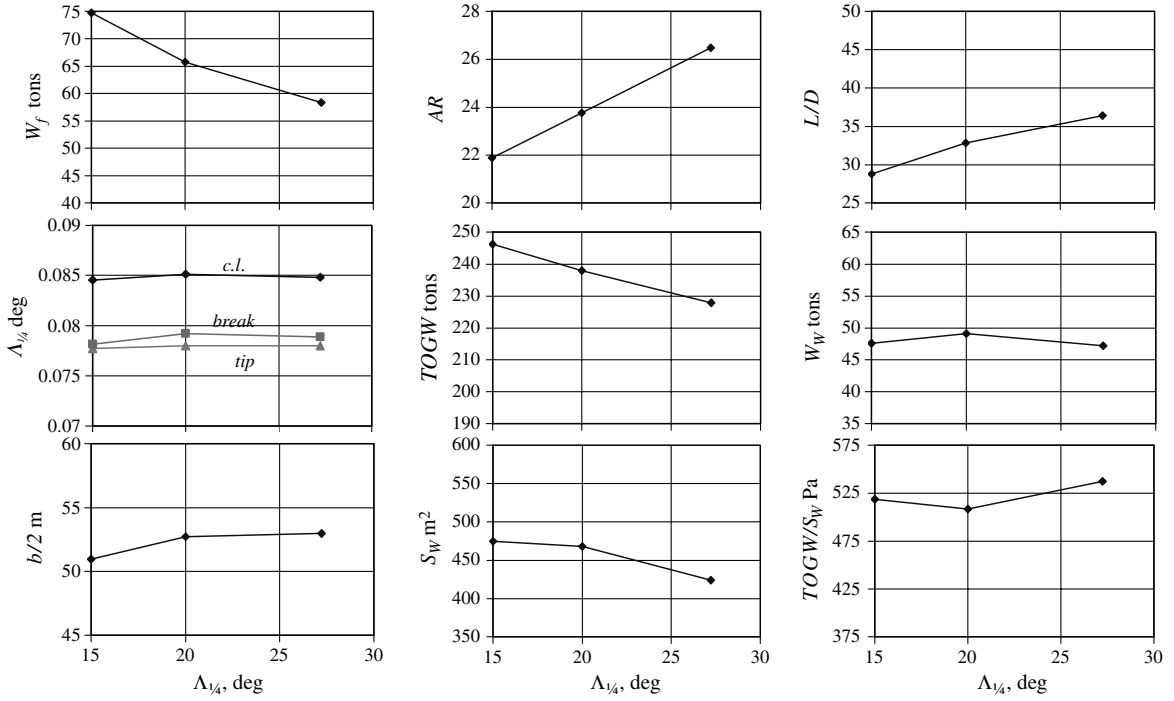

Fig. 17 Quarter-chord sweep-angle study, key parameters.

D. Maximum 2-D Cruise Lift Coefficient Influence

Figure 24 shows the optimized configurations for three different maximum 2-D cruise lift coefficients: $C_{l,\max} = 0.6$, 0.8 (baseline), 1.0, and Fig. 25 presents the dependency of the design parameters on that parameter. For the $C_{l,\max} = 0.6$ and 0.8 designs, the active constraints are the range and the maximum 2-D cruise lift coefficient, but for the $C_{l,\max} = 1.0$ design the active constraints are the range, fuel volume, and approach speed. The fuel volume constraint becomes active due to the lower wing chords, and the approach speed constraint is active due to the increased wing loading.

As the maximum 2-D cruise lift coefficient is increased, the fuel weight is decreased. The wing aspect ratio is increased with $C_{l,\max}$; thus, the wing chord is decreased, enabling the local cruise lift coefficient to increase. Observe that the lift-to-drag ratio remains practically constant. The decreased chord enables a higher laminar chordwise ratio, which reduces the friction drag (see Fig. 26). Increased local cruise lift coefficient causes higher wing sweep, which maintains a similar wave drag. This can be directly concluded from the Korn equation [19]:

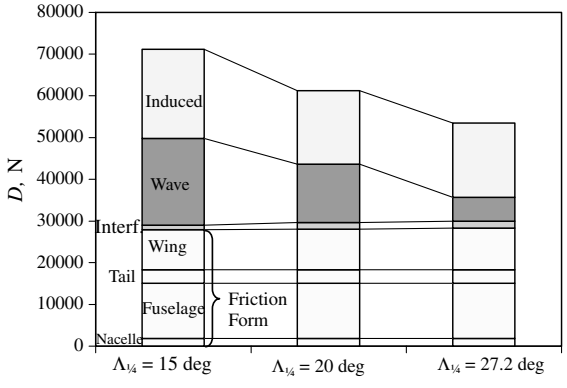

Fig. 18 Quarter-chord sweep-angle study, drag breakdown.

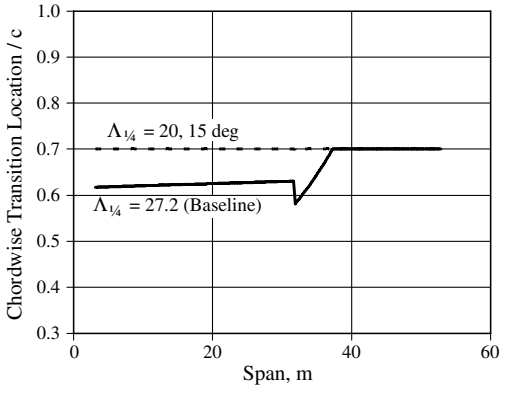

Fig. 19 Quarter-chord sweep-angle study, main wing chordwise transition location.

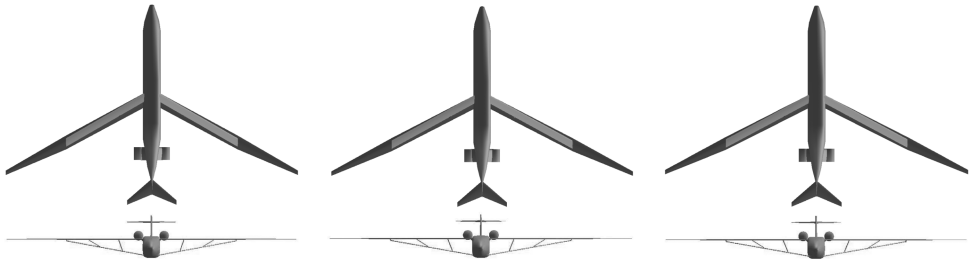

a) $\%c_{max,laminar} = 40$ b) $\%c_{max,laminar} = 70$ (baseline) c) $\%c_{max,laminar} = 100$

Fig. 20 Maximum chordwise laminar extent ratio study, configurations.

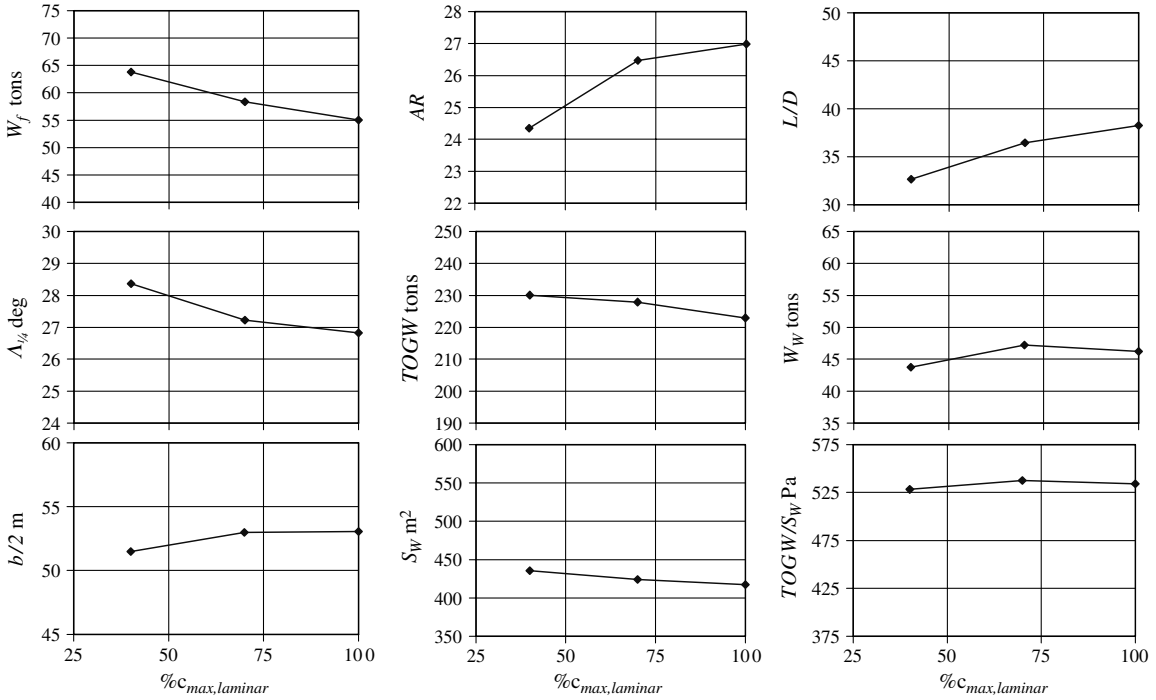

Fig. 21 Maximum chordwise laminar extent ratio study, key parameters.

$$M_{DD} \cdot \cos \Lambda_{1/2} + \frac{C_l}{10 \cdot \cos^2 \cdot \Lambda_{1/2}} + \frac{t/c}{\cos \Lambda_{1/2}} = K_A \qquad (4)$$

For a given Korn factor K_A, drag divergence Mach number M_{DD}, and thickness-to-chord ratio t/c, as the local cruise lift coefficient C_l is increased, and the midchord sweep angle $\Lambda_{1/2}$ increases as well. Figure 26 shows that the final design results in a decreased wave drag for higher $C_{l,\max}$.

The 2-D cruise lift coefficient distributions for the wing, main strut, and horizontal tail are presented in Fig. 27. The aerodynamic loading is trimmed around the vehicle center of gravity; thus, the horizontal tail loading is negative. As shown in Fig. 27, the maximum cruise lift coefficient is reached on the inner part of the main wing. The difference between the $C_{l,\max} = 0.8$ design and the $C_{l,\max} = 1.0$ design is small, and this occurs because the maximum 2-D cruise lift coefficient constraint is no longer active for the $C_{l,\max} = 1.0$ case.

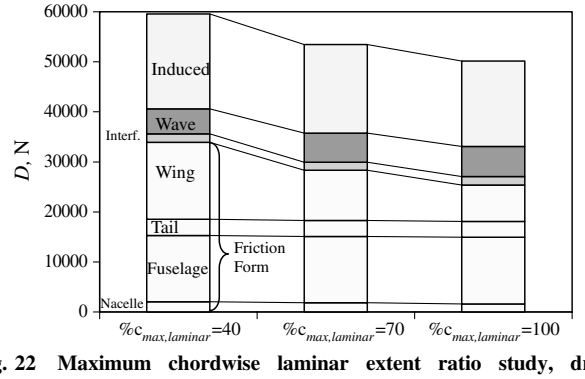

Fig. 22 Maximum chordwise laminar extent ratio study, drag breakdown.

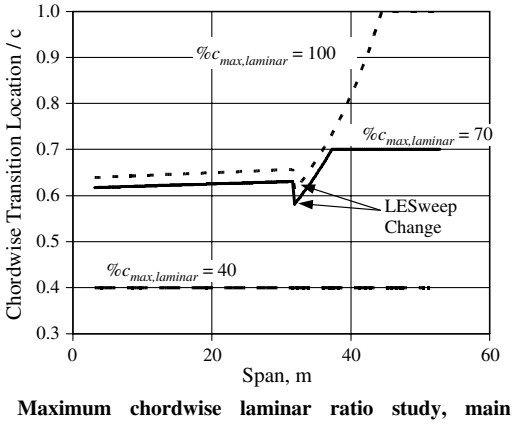

Fig. 23 Maximum chordwise laminar ratio study, main wing chordwise transition location.

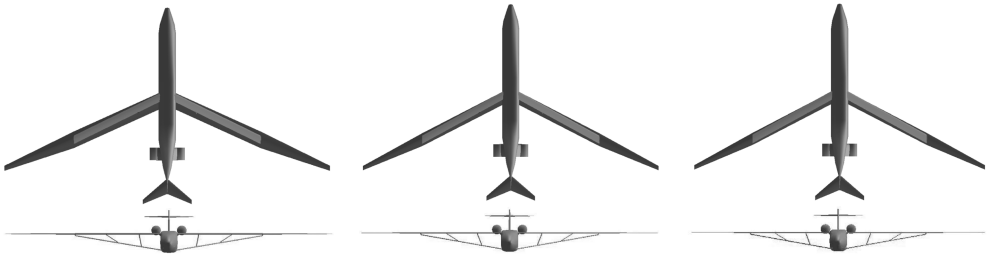

a) $C_{l,max}$ = 0.6 b) $C_{l,max}$ = 0.8 (baseline) c) $C_{l,max}$ = 1.0

Fig. 24 Maximum 2-D cruise lift coefficient study, configurations.

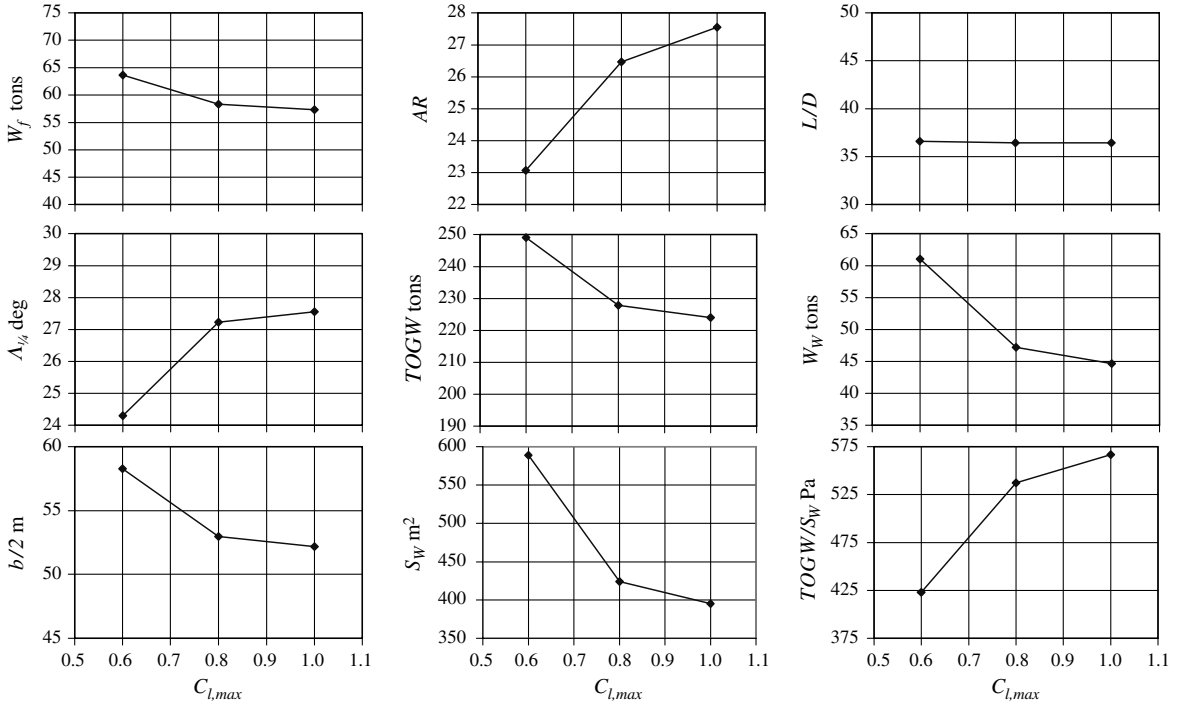

Fig. 25 Maximum 2-D cruise lift coefficient study, key parameters.

E. Korn-Factor Influence

As discussed in the previous section, the Korn factor has a significant role in the wave-drag model. Figure 28 shows the optimized configurations for three different Korn factors: $K_A = 0.87$, 0.91, and 0.95 (baseline). The active constraints for the three configurations are the range and the maximum 2-D cruise lift coefficient. For the $K_A = 0.87$ design, the fuel capacity constraint is active as well due to the increased fuel weight.

Figure 29 illustrates the dependency of the design parameters with the Korn factor. It is clear that as the Korn factor is decreased, the wing sweep is increased, span is decreased, and the fuel weight is increased. All of the above relate to the decreased wave drag (see Fig. 30) as the airfoil supercritical properties are improved (higher Korn factor). The wing sweep of a fully supercritical airfoil ($K_A = 0.95$) is 27 deg, and for a conventional airfoil ($K_A = 0.87$) the wing sweep is 38 deg. As points of reference, one can refer to the conventional-airfoil Boeing 707, which has a sweep angle of 35 deg, and to the supercritical-airfoil Boeing 777 (31.6 deg) and Boeing 787 (32.2 deg); both are marked in Fig. 29.

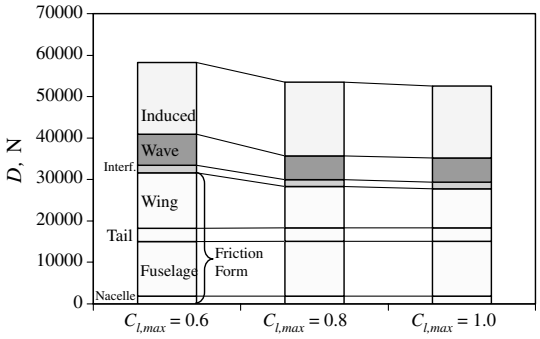

Fig. 26 Maximum 2-D cruise lift coefficient study, drag breakdown.

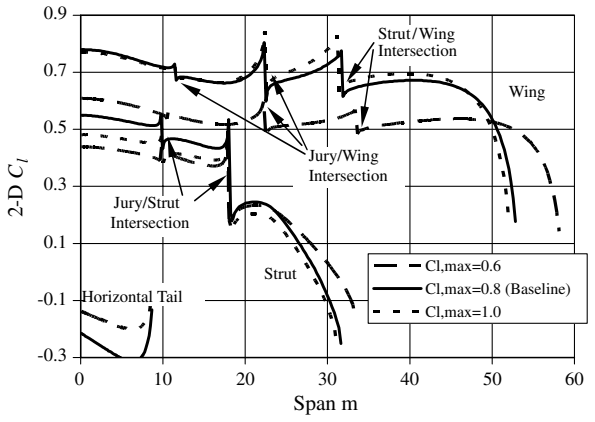

Fig. 27 Maximum 2-D cruise lift coefficient study, loading distribution.

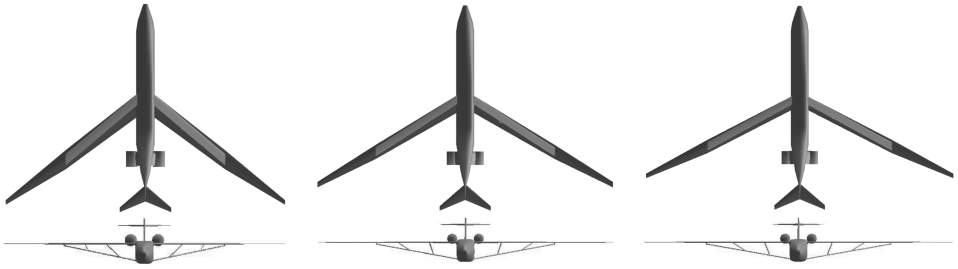

a) $K_A = 0.87$ b) $K_A = 0.91$ c) $K_A = 0.95$ (baseline)

Fig. 28 Korn-factor study, configurations.

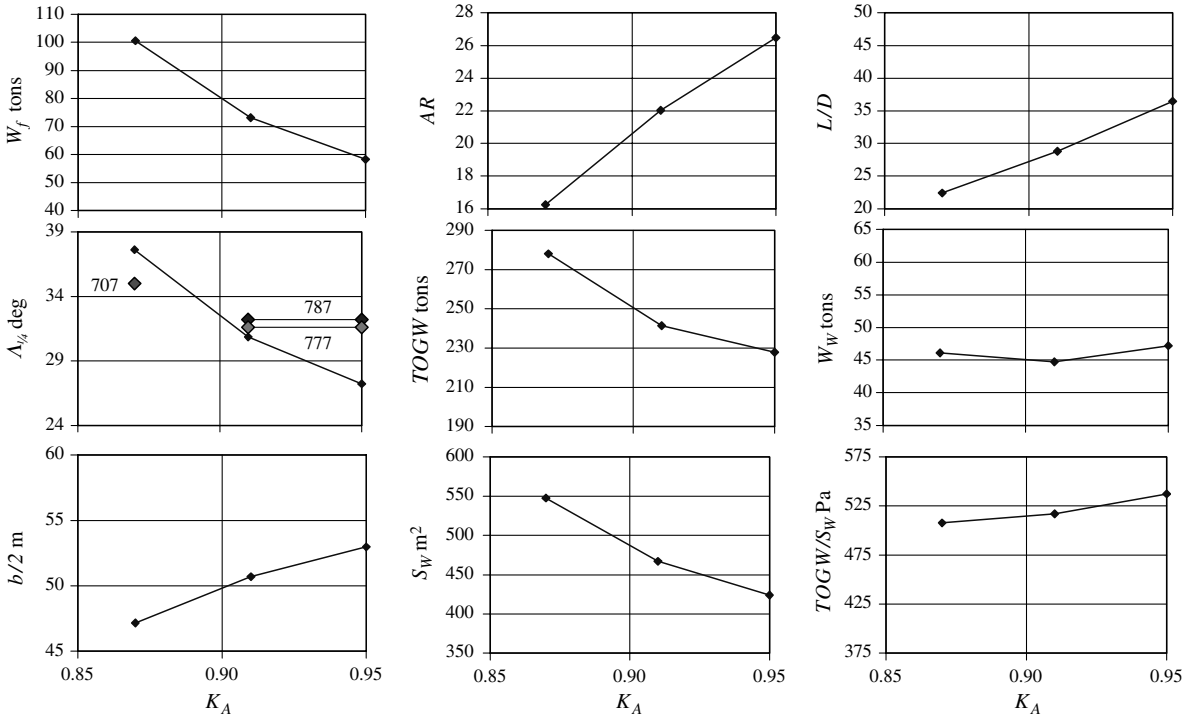

Fig. 29 Korn-factor study, key parameters.

As the Korn factor is increased, the friction drag is decreased (see Fig. 30). The lower sweep angle and lower chords permit an increased use of NLF.

All of the above emphasize the importance of airfoil design. The authors are aware of the conflicting criteria for such an airfoil design: supercritical, laminar, low drag, and high lift [43].

F. Cruise Mach Number Influence

The usual assumption relating to the cruise Mach number is that as it decreases, the vehicle drag decreases due to decreased wave drag. This has influenced several researchers to pursue lower cruise Mach designs [1]. To explore the validity of this assumption, a design study was performed using different cruise Mach numbers. Because of the close interaction of the cruise Mach number and altitude, two studies were conducted. One used a constant cruise altitude of $H_{cr} = 14,630$ m (48,000 ft), and the second used the cruise altitude H_{cr} as a design variable. For that case, as the Mach number is decreased the cruise altitude is decreased (see Fig. 31).

Figure 32 shows the optimized configuration for three different cruise Mach numbers: $M = 0.75, 0.80, 0.85$ (baseline). The active constraints for all configurations are the range and maximum 2-D cruise lift coefficient. Figure 33 presents the dependency of the design parameters on the cruise Mach number.

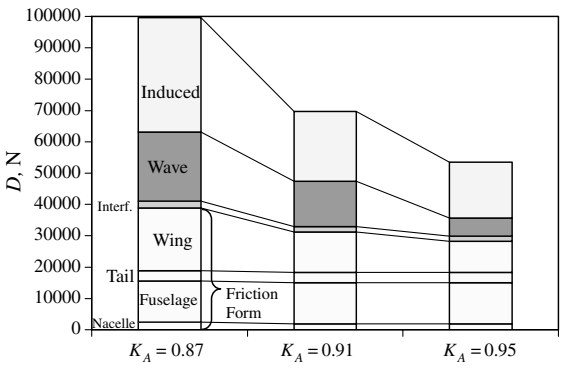

Fig. 30 Korn-factor study, drag breakdown.

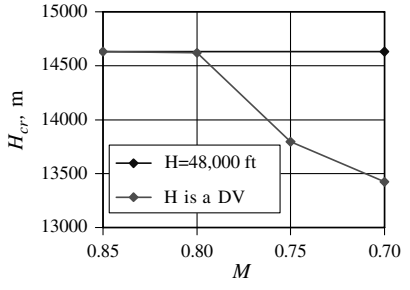

Fig. 31 Cruise Mach number study, cruise altitude.

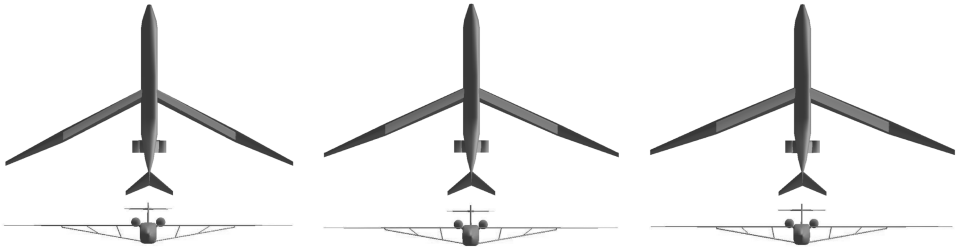

a) $M = 0.85$ (baseline) b) $M = 0.80$ c) $M = 0.75$

Fig. 32 Cruise Mach number study, configurations.

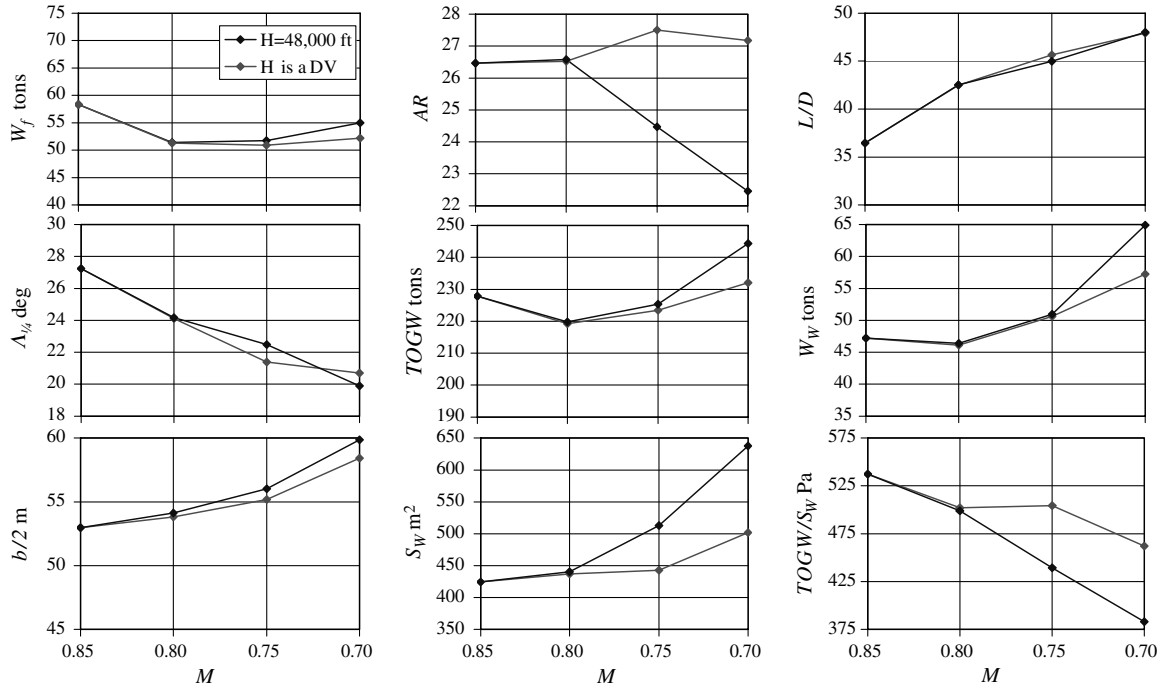

Fig. 33 Cruise Mach number study, key parameters.

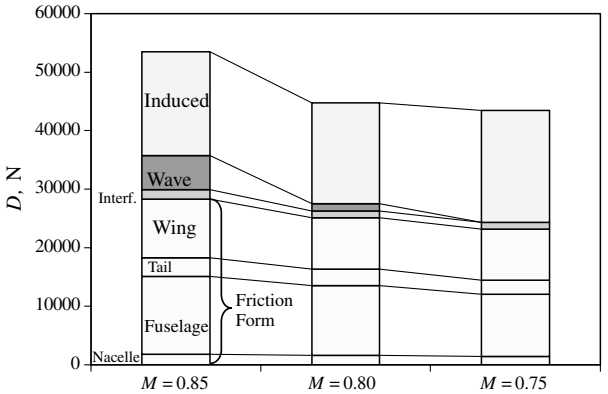

Fig. 34 Cruise Mach number study, drag breakdown.

The wave-drag reduction is noticeable as the Mach number decreases (see Fig. 34), but it is accompanied by an increased wing area. This increased wing area keeps the 3-D cruise lift coefficient, C_L, low, although the dynamic pressure is decreased. When the cruise altitude is used as a design variable, in addition to the increased wing area the cruise altitude is decreased. Still, the same trends exist; thus, when the cruise altitude is decreased due to the decreased Mach number, the wing area is increased. These trends were already presented in [39].

The increased wing area causes an increased wing weight, which then influences the vehicle TOGW. This is the reason that although the drag is reduced as the Mach number is decreased, there is a minimum-fuel point that results in an optimized Mach number. For the current case, the lowest fuel consumption is reached for $0.75 < M < 0.8$. For $M < 0.75$ the increased wing weight

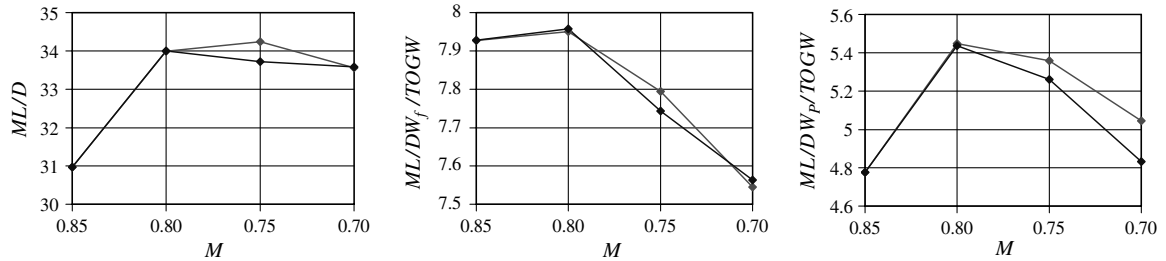

Fig. 35 Cruise Mach number study, cruise figures of merit.

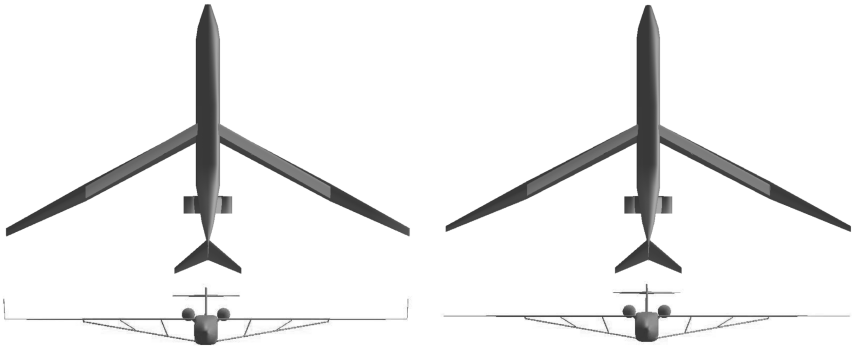

a) With winglets b) Without winglets

Fig. 36 Winglet influence, configurations.

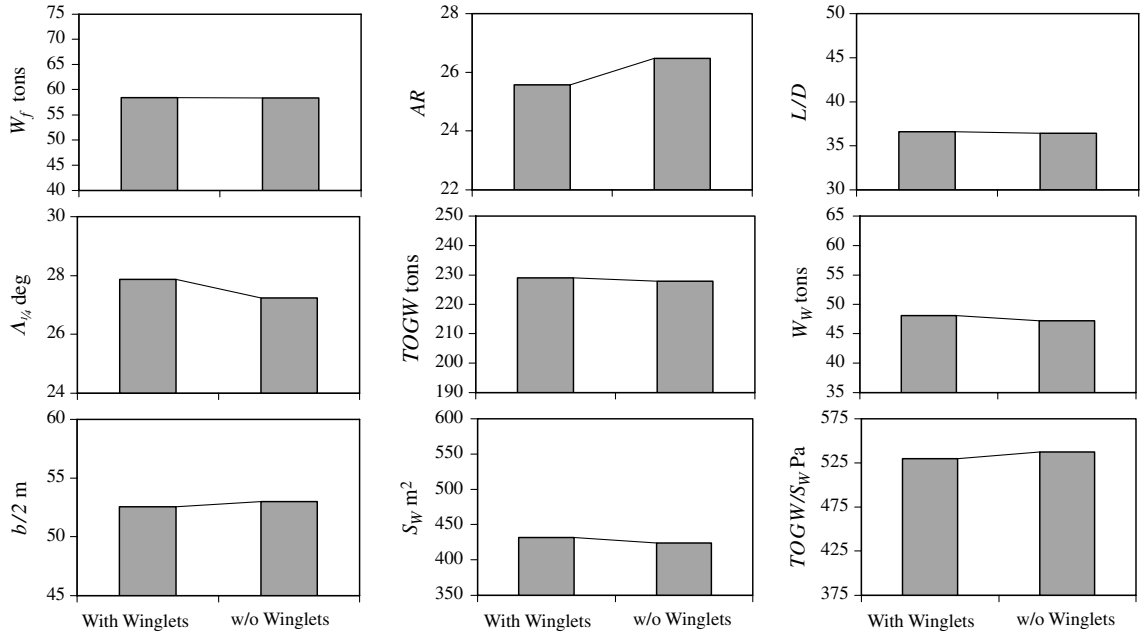

Fig. 37 Winglet influence study, key parameters.

overcomes the reduced drag, and as the Mach number is decreased the vehicle efficiency is reduced.

The reduced Mach number causes a reduction of the wing sweep, while the wave drag is decreased. The lower sweep angle, lower cruise Mach number and increased wing area, keep the wing friction drag almost the same. The fuselage friction drag is decreased due to the lower airspeed, and the induced drag is increased due to the higher vehicle weight (see Fig. 34).

It is clear that the total drag is decreased as the cruise Mach number is decreased, but using MDO techniques reveals counter-influences leading to increased vehicle weight. Figure 35 shows three different range figures of merit: ML/D, $ML/D\,(W_f/\text{TOGW})$, and $ML/D\,(W_p/\text{TOGW})$, where W_p is the payload weight. These three parameters exhibit the same optimum Mach number; thus, they also reflect the equilibrium between the vehicle drag and wing weight.

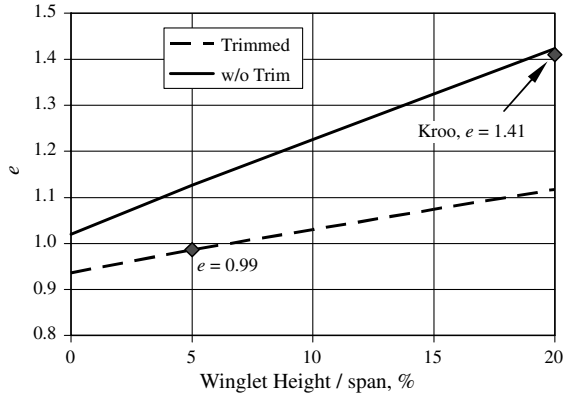

Fig. 38 Winglet influence study, drag breakdown.

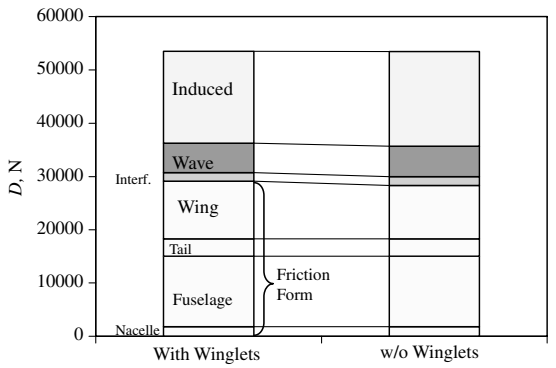

Fig. 39 Wing-tip influence study, Oswald coefficient for different winglet heights.

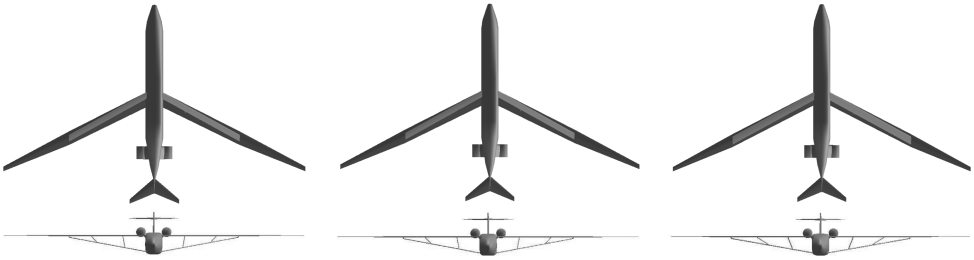

a) $C_{Fairing} = 0.2$ b) $C_{Fairing} = 0.1$ c) $C_{Fairing} = 0.02$

Fig. 40 Fairing-factor study, configurations.

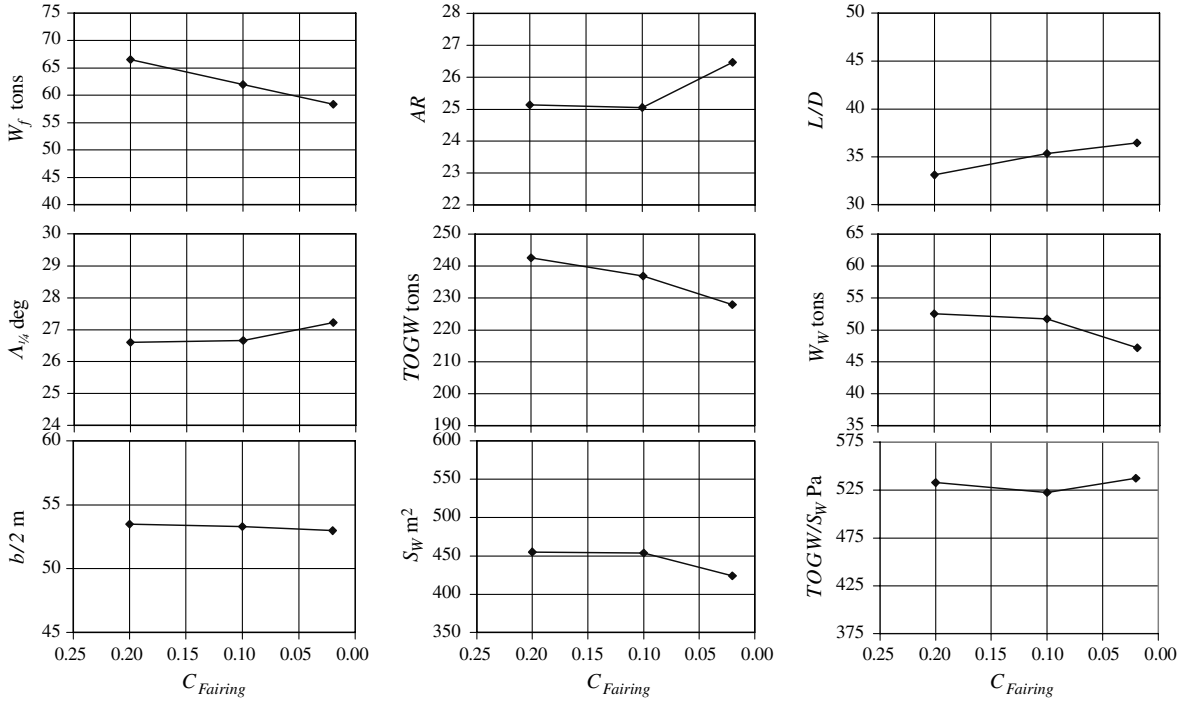

Fig. 41 Fairing-factor study, key parameters.

G. Wing-Tip-Treatment Influence

A common means for induced-drag reduction are wing-tip installations. To explore the influence of wing-tip treatments, simple vertical winglets were considered. Kroo compared several nonplanar wings and showed that vertical winglets are comparable to C-wings and box wings [44]. Thus, for vertical winglets, the potential of induced drag reduction is high. The winglet length is set to 5% of the wingspan, which for the optimized configuration is 5 m (17 ft). Figure 36 shows the optimized configuration for two different configurations: with and without (baseline) winglets. Figure 37 presents the design parameters for these two configurations.

The Oswald efficiency coefficient e for the baseline configuration is $e = 0.93$, and for the winglet configuration it is $e = 0.99$. Recall that the trim drag is included in these calculations. Analysis of the same configurations without the trim process results in an Oswald coefficient of $e = 1.02$ for the baseline configuration, and $e = 1.13$ for the wing-tip configuration. Kroo [44] showed that for vertical winglets with 20% span length, the Oswald coefficient is $e = 1.41$. For 20% span-length wing tip, the optimized configuration results in a trimmed $e = 1.12$ and an untrimmed $e = 1.42$ (Fig. 38). Note that 20% span for this configuration is 21.2 m (69 ft), which is probably impractical.

The difference between fuel weight for the two configurations is negligible. The use of winglets reduces the vehicle induced drag, but increases the friction drag due to the increased wetted area (see Fig. 39); thus, the total drag of the two configurations is similar.

The use of winglets is based on the assumption that the induced drag is reduced while the span remains the same or even decreases; thus, the wing bending moment remains the same as well and the wing weight is not increased. This is true for a given vehicle that was already designed with planar wings and then the winglets were added. As demonstrated here, for a new design, the use of winglets is not beneficial.

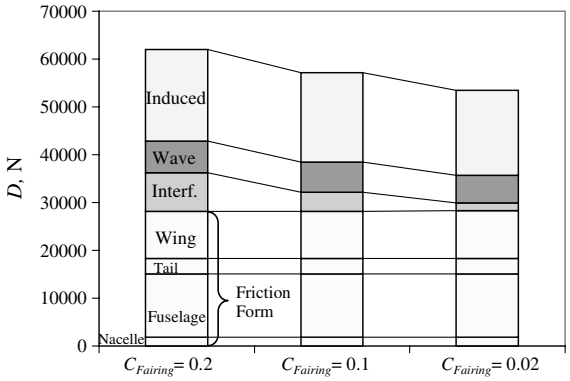

Fig. 42 Fairing-factor study, drag breakdown.

a) $L_{laminar}/L_{fuselage} = 0.01$ b) $L_{laminar}/L_{fuselage} = 0.5$ c) $L_{laminar}/L_{fuselage} = 0.75$

Fig. 43 Fuselage relaminarization study, configurations.

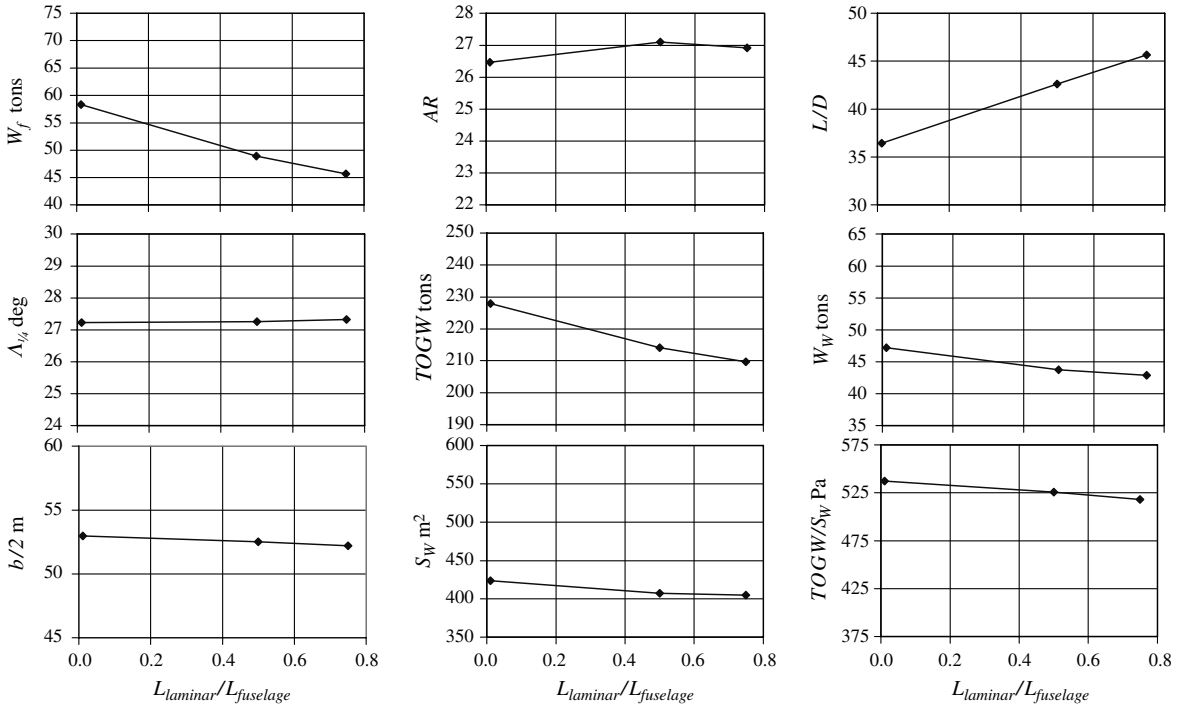

Fig. 44 Fuselage relaminarization study, key parameters.

H. Fairing-Factor Influence

The intersection drag is found from data for unfaired wings intersections. It is possible to design an effective fairing; thus, the interference drag can be reduced dramatically and in some cases eliminated. The fairing factor C_{fairing} is applied to the unfaired calculated interference drag; thus, it represents a fairing efficiency, except that low values are better.

Figure 40 shows the optimized configurations for three different fairing factors: $C_{\text{fairing}} = 0.2$, 0.1, and 0.02 (baseline). The use of $C_{\text{fairing}} = 0.2$ is very pessimistic, and $C_{\text{fairing}} = 0.1$ represents a conventional intersection design. For the entire range of fairing factor, the active constraints are the range and maximum 2-D cruise lift coefficient. The front view shows that as the fairing factor increases the jury truss members become more vertical; thus, the intersection angles approach normal.

Figure 41 presents the design parameters for these configurations. As the fairing factor is increased, the fuel weight is increased due to the increased interference drag (see Fig. 42), while the other drag components remain practically the same.

I. Fuselage Relaminarization Influence

One of the ways to reduce the fuselage friction drag is to use relaminarization. By sucking the turbulent boundary layer after the cockpit and entrance doors, one can cause parts of the fuselage to experience laminar conditions. Figure 43 shows the optimized configuration for three different fuselage laminar length ratios, $L_{\text{laminar}}/L_{\text{fuselage}} = 0.01$ (baseline), 0.5, and 0.75. Active constraints for all configurations are the range and maximum 2-D cruise lift coefficient.

Figure 44 presents the design parameters for these configurations, and Fig. 45 shows the drag breakdown. As expected, the main impact of increased laminar length ratio is a reduction of the fuselage friction/form drag. This drag-reduction results in sharply higher

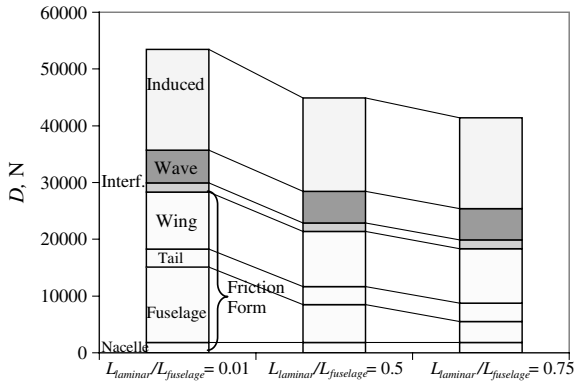

Fig. 45 Fuselage relaminarization study, drag breakdown.

a) $\Delta C_{f,turbulent} = 0\%$ b) $\Delta C_{f,turbulent} = 5\%$ c) $\Delta C_{f,turbulent} = 7\%$

Fig. 46 Riblet turbulent skin-friction-reduction study, configurations.

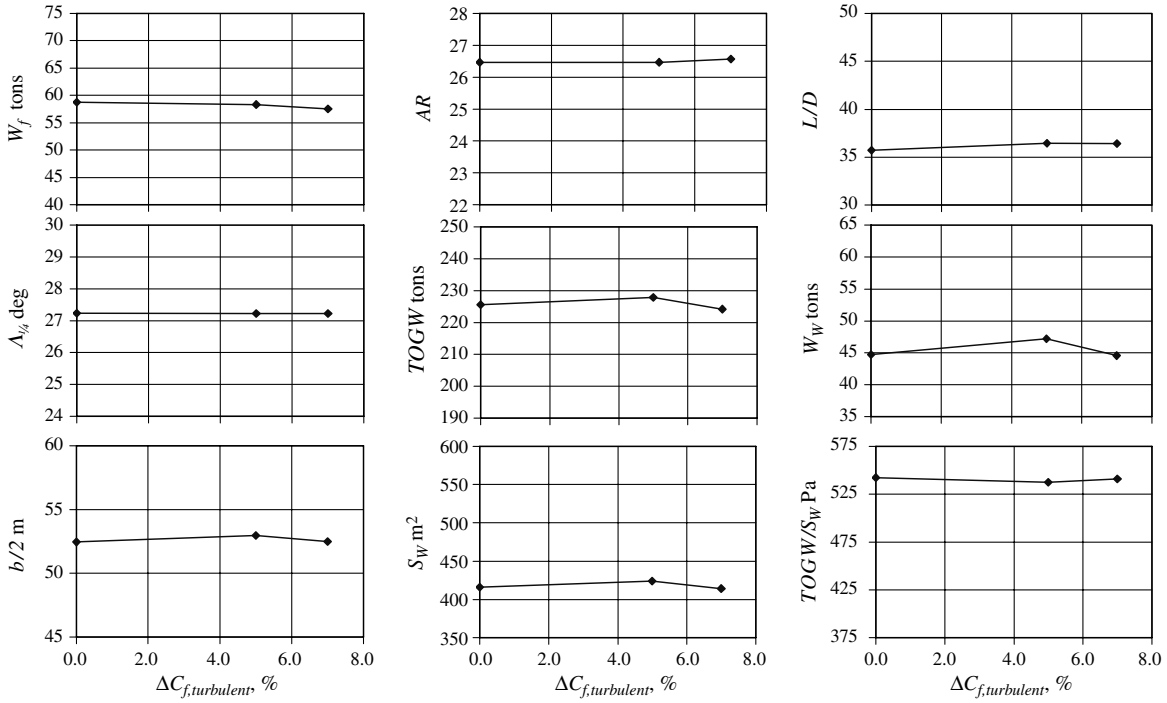

Fig. 47 Riblet turbulent skin-friction-reduction study, key parameters.

lift-to-drag ratio, lower fuel weight, and lower TOGW. Note that the wing planform does not change significantly for different fuselage laminar length ratios.

J. Fuselage Turbulent Skin-Friction Reduction with Riblets' Influence

A different way to reduce the fuselage friction/form drag is by using riblets, which reduce the turbulent skin friction $\Delta C_{f,\text{turbulent}}$. Figure 46 shows the optimized configurations for three different fuselage riblet turbulent skin-friction reductions: $\Delta C_{f,\text{turbulent}} = 0\%$, 5% (baseline), and 7%. All of these configurations share the same active constraints: range and maximum 2-D cruise lift coefficient.

Figure 47 presents the design parameters for these configurations. Comparing Figs. 44 and 47 reveals that the influence of the riblets on the fuel consumption is small compared with other techniques such as fuselage relaminarization. Note that this study does not include any weight or cost penalty due to riblet installation. However, some claim that the weight and cost of riblets is about the same as paint. As in the fuselage relaminarization influence study, the main influence of the riblets is on the fuselage friction drag while the other drag components remain almost constant (see Fig. 48).

K. Goldschmied-Factor Influence

A third possibility to reduce the fuselage friction/form drag is with the Goldschmied apparatus. Figure 49 shows the optimized configuration for three different values of the Goldschmied factors: $C_{\text{Goldschmied}} = 0.0$ (baseline), 0.5, and 1.0 (see Sec. V, item 10, for an explanation). All configurations share the same active constraints: range and maximum 2-D cruise lift coefficient.

Figure 50 presents the design parameters for these configurations, and Fig. 51 shows the drag breakdown. As in the previous two sections, which dealt with fuselage friction/form drag reduction, most of the vehicle geometry parameters do not change significantly. The vehicle drag is reduced, lift-to-drag ratio is increased, and, as a

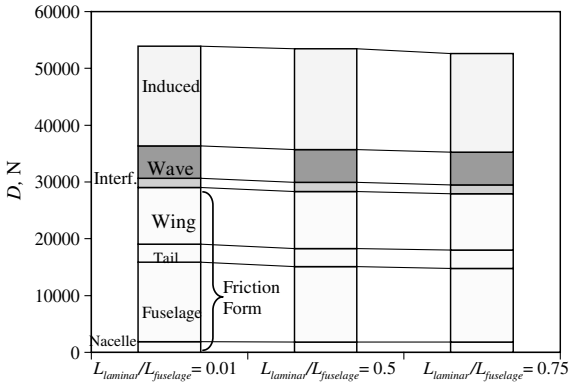

Fig. 48 Riblet turbulent skin-friction-reduction study, drag breakdown.

a) $C_{Goldschmied} = 0.0$ b) $C_{Goldschmied} = 0.5$ c) $C_{Goldschmied} = 1.0$

Fig. 49 Goldschmied-factor study, configurations.

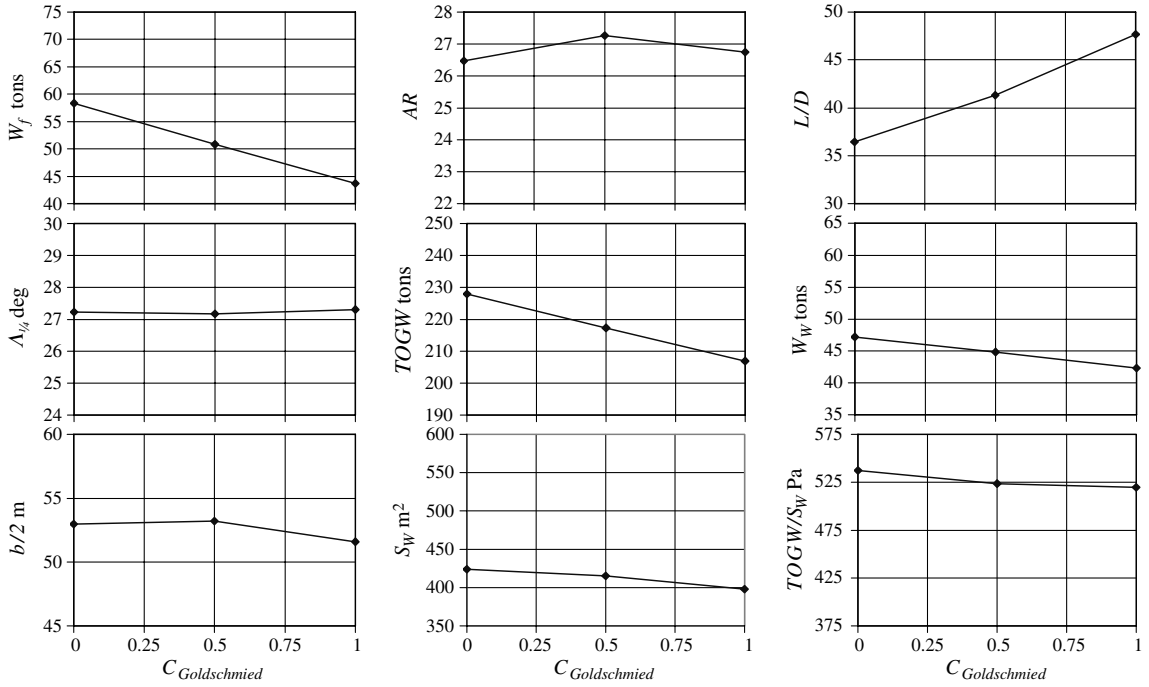

Fig. 50 Goldschmied-factor study, key parameters.

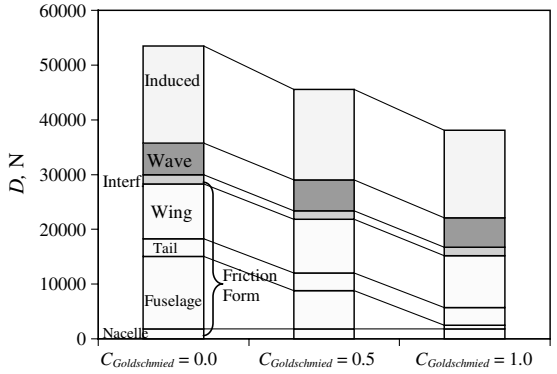

Fig. 51 Goldschmied-factor study, drag breakdown.

consequence, the fuel weight is reduced. The fuel weight reduction is similar to that in the fuselage relaminarization study and much higher than in the riblets study. Note that any weight penalty due to the Goldschmied apparatus is not available and is thus not taken into account here, so these results should be considered as optimistic.

L. Influence of Tailless and Tailless-Plus-Goldschmied Configurations

One can envision a tailless configuration with thrust-vector control from the engine nozzles. The aim is to reduce the tail drag. Further, the Goldschmied apparatus might be combined with a thrust-vectoring concept, and the combination of the two technologies can result in substantial fuel reduction. Figure 52 shows the optimized configuration of fuselage buildup of the baseline, tailless, and

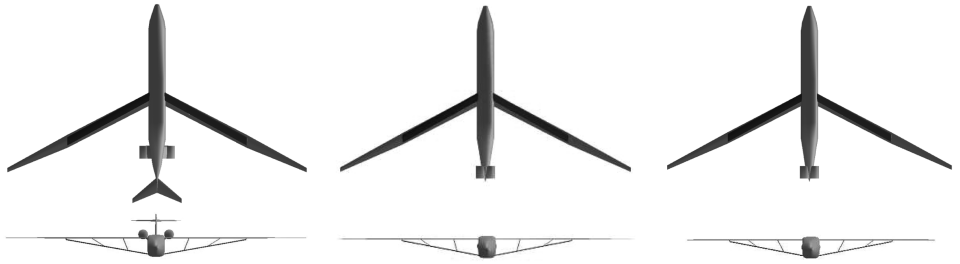

a) Baseline b) Tailless c) Tailless + Goldschmied

Fig. 52 Fuselage buildup study, configurations.

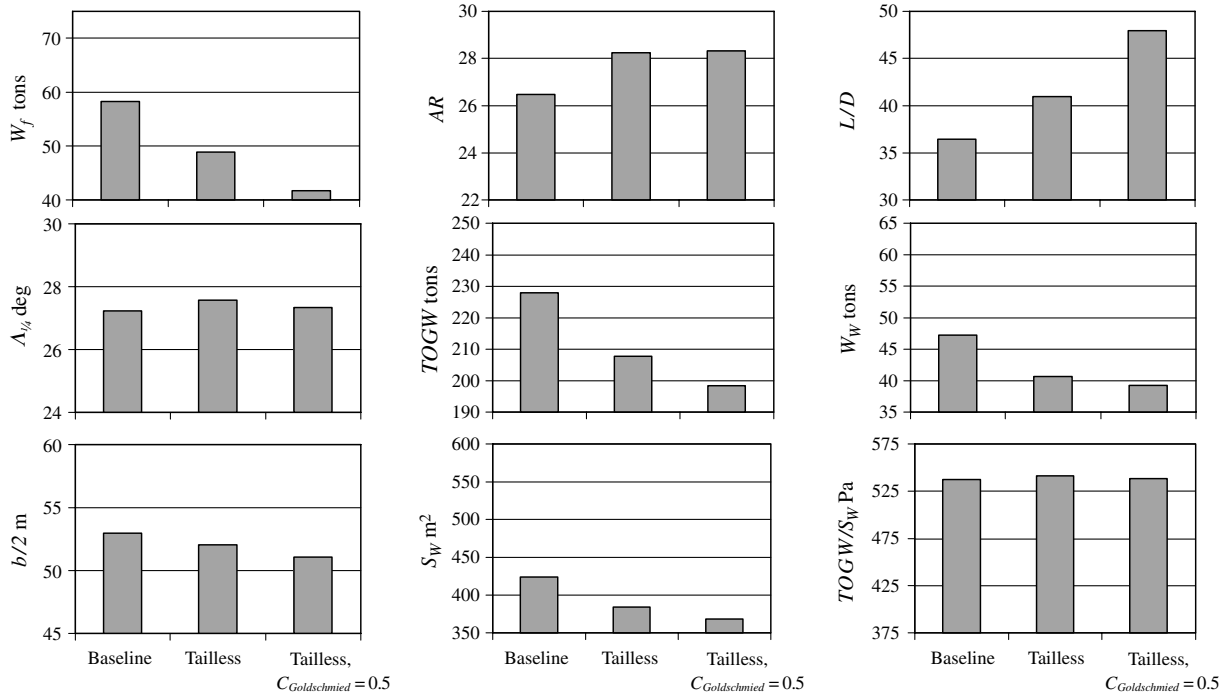

Fig. 53 Fuselage buildup study, key parameters.

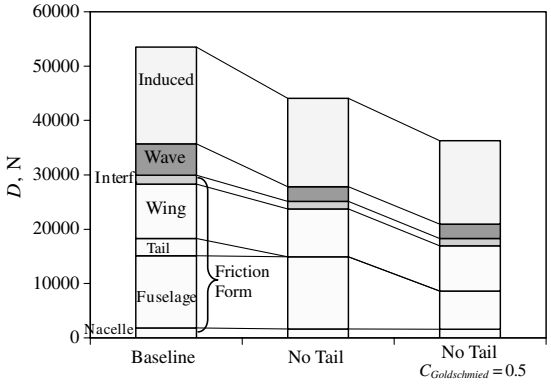

Fig. 54 Fuselage buildup study, drag breakdown.

tailless-plus-Goldschmied coefficient $C_{\text{Goldschmied}} = 0.5$ designs. All configurations have the same active constraints: range and maximum 2-D cruise lift coefficient.

Note that the tailless configuration is aerodynamically trimmed; thus, no additional penalty is introduced to the thrust, which is produced by propulsion system. As in the previous studies, no weight penalties are considered here due to the thrust vectoring or the Goldschmied apparatus.

Figure 53 presents the design parameters for these configurations. The tailless configuration eliminates the tail wave and friction/form drag (see Fig. 54). This results in substantial fuel weight reduction. Adding the Goldschmied apparatus enables further reduction of the fuel weight. This buildup does not change the wing loading significantly, whereas the TOGW decreases; thus, the wing area decreases as well and the wing aspect ratio increases.

VI. Conclusions

Several trend studies are described in this paper. The baseline design is a two-jury truss-braced-wing long-range transport aircraft that was designed using aggressive natural laminar flow and has a conventional fuselage, empennage, and engines. In all cases, the minimum-fuel/emissions optimum design was sought. Each study focused on a specific aerodynamic parameter that represents a different technology. Two combined effect studies were also conducted.

The first group of technologies considered relates to the lifting-surface aerodynamic properties and results, with the following conclusions:

1) As the natural-laminar-flow technology factor is increased, the fuel weight is decreased, due to the increased extent of laminar flow. This is accompanied with increased lift-to-drag ratio and increased aspect ratio. The influence of the laminar technology factor on the wing sweep is small due to the counterbalance of the wave drag.

2) As the quarter-chord sweep is decreased, the L/D is decreased because the wave drag goes up sharply and the friction drag hardly changes. The gain in NLF at lower sweep angles is only to maintain laminar flow up to the 70% limit over the whole wing, compared with 60% in the inboard region of the wing for the baseline design.

3) The maximum chordwise laminar extent limit has a distinct impact on the vehicle geometry. As the chordwise limit is increased, the wing chord is reduced, aspect ratio is increased and the lift-to-drag ratio is increased. All of these trends result in a decreased fuel weight. The chordwise transition extent ratio limitation is an important parameter, which together with TF establishes the laminar properties of the wing. The use of a high laminar technology factor with a low maximum chordwise laminar extent limit does not enable full exploitation of NLF potential.

4) As the maximum 2-D cruise lift coefficient is increased, the fuel weight is decreased. The wing aspect ratio is increased with the maximum 2-D cruise lift coefficient; thus, the wing chord is decreased, enabling the local cruise lift coefficient to increase. This happens while the lift-to-drag ratio remains practically constant.

5) As the Korn factor is increased, the wing sweep is decreased, span is increased, and the fuel weight is increased. All of the above relate to the decreased wave drag as the airfoil supercritical properties are improved (higher Korn factor). This emphasizes the critical importance of airfoil design. The wing sweep of a fully supercritical airfoil ($K_A = 0.95$) is 27 deg, and for a conventional airfoil ($K_A = 0.87$) the wing sweep is 38 deg.

6) Decreased cruise Mach number reduces the wave drag but causes an increased wing area. This is the reason that although the drag is reduced as the Mach number is decreased, there is a point that results in a minimum-fuel Mach number. For the current case, the lowest fuel consumption is reached for $0.75 < M < 0.8$.

7) The use of winglets reduces the vehicle induced drag, but increases the friction drag due to the increased wetted area; thus, the total drag of the two configurations is similar. The use of winglets is based on the assumption that the induced drag is reduced for a given wing weight. This is true for a given vehicle that has already been designed with a planar wing or where a span constraint exists. For these cases, additional wing tips might be beneficial. As demonstrated here, for a new design, the use of winglets is not beneficial. Note that although a gate-box limit of 80 m is used, the span in the current effort is not constrained due to the assumed use of a folding-wing mechanism.

8) As the fairing factor increases (less effective fairing) the jury truss members become more vertical; thus, the intersection angles approach normal angles. In addition, the fuel weight is increased due to the increased interference drag, while the other drag components remain practically the same.

The second group of case studies relates to the aerodynamic technologies of the fuselage results, with the following conclusions:

1) Increased laminar length ratio reduces the fuselage friction drag. This drag-reduction results in sharply higher lift-to-drag ratio, lower fuel weight, and lower TOGW. The wing planform does not change significantly for different fuselage laminar length ratios.

2) The riblets' effect on fuel consumption is small compared with other techniques such as fuselage relaminarization. The main influence of the riblets is on the fuselage friction drag, while the other drag components remain almost constant.

3) With a Goldschmied apparatus, most of the vehicle geometry parameters do not change significantly. The vehicle drag is reduced, lift-to-drag ratio is increased, and, as a consequence, the fuel weight is reduced. Careful studies of the Goldschmied concept in transonic flow are needed. Note that the study presented here does not consider any weight penalty due to the Goldschmied device.

4) The tailless configuration eliminates the tail wave and friction/form drag.

This results in substantial fuel weight reduction. Adding the Goldschmied apparatus enables further reduction of the fuel weight. This buildup does not change the wing loading significantly, while the TOGW decreases; thus, the wing area decreases as well and the wing aspect ratio increases.

The study presented here shows that the TBW concept is considerably better than a conventional wing configuration. Using the truss system, the wing can have an increased span and aspect ratio, while the structural weight is kept the same or lower. This activates the two-dimensional cruise lift coefficient constraint due to the decreased chord length.

With the increased aspect ratio, the importance of the two-dimensional airfoil section is increased; thus, the maximum benefit requires superior airfoil design technology. The design criteria present a challenge to the airfoil designer and include a swept, NLF wing, excellent supercritical characteristics, high design lift coefficient, and low drag.

In all cases studied, the wings continue to be swept. This is true also for a combination of low Mach number and high Korn factor. The benefit of an unswept wing due to higher laminar flow is overcome by the wave drag, which tries to increase the wing sweep.

One of the key ways to reduce the vehicle drag and improve its efficiency is treating the fuselage drag. This may reduce dramatically the vehicle fuel consumption along with emissions. This is especially true for a low induced drag design with NLF like TBW, but this conclusion is applicable also for a conventional aircraft configuration.

Acknowledgments

The authors would like to acknowledge the financial support of NASA Langley Research Center with Vivek Mukhopadhyay as Technical Monitor. Chief Scientist Dennis Bushnell inspired our efforts. The authors thank Rakesh Kapania and Manav Bhatia from Virginia Polytechnic Institute and State University, Department of Aerospace and Ocean Engineering, and Taewoo Nam and Hongjun Ran from Georgia Institute of Technology, Daniel Guggenheim School of Aerospace Engineering. They all supported our efforts.

References

[1] Warwick, G., "Future Shaping," *Aviation Week and Space Technology*, Vol. 172, No. 19, 17 May 2010, pp. 40–42.

[2] Gur, O., Bhatia, M., Schetz, J. A., Mason, W. H., Kapania, R. K., and Mavris, D., "Multidisciplinary Design Optimization of Truss Braced Wing Aircraft," 9th AIAA Aviation Technology, Integration, and Operations Conference and Aircraft Noise and Emissions Reduction Symposium, AIAA Paper 2009-7114, Hilton Head, SC, Sept. 2009.

[3] Goldschmied, F. R., "Fuselage Self-Propulsion by Static-Pressure Thrust: Wind-Tunnel Verification," AHS, and ASEE, Aircraft Design, Systems and Operations Meeting, AIAA Paper 1987-2935, Saint Louis, MO, Sept. 1987.

[4] Pfenninger, W., "Laminar Flow Control Laminarization," *Special Course on Concepts for Drag Reduction*, AGARD Rept. 654, Neuilly-sur-Seine, France, Jan. 1976.

[5] Grasmeyer, J. M., "Multidisciplinary design optimization of a transonic strut-braced wing aircraft," 37th AIAA Aerospace Sciences Meeting and Exhibit, AIAA Paper 1999-0010, Reno, NV, Jan. 1999.

[6] Gundlach, J. F., IV, Tétrault, P.-A., Gern, F. H., Nagshineh-Pour, A. H., Ko A. Y-Y., Schetz, J. A., Mason, W. H., Kapania, R. K., Grossman, B., and Haftka, R. T., "Conceptual Design Studies of a Strut-Braced Wing Transonic Transport," *Journal of Aircraft*, Vol. 37, No. 6, Nov.–Dec. 2000, pp. 976–983. doi:10.2514/2.2724

[7] Gern, F. H., Ko, A. Y-Y., Grossman, B., Haftka, R. T., Kapania, R. K., Mason, W. H., and Schetz, J. A., "Transport Weight Reduction Through MDO: The Strut-Braced Wing Transonic Transport," 35th AIAA Fluid Dynamics Conference and Exhibit, AIAA Paper 2005-4667, Toronto, June 2005.

[8] Duggirala, R. K., Roy, C. J., and Schetz, J. A., "Analysis of Interference Drag for Strut-Strut Interaction in Transonic Flow," 47th AIAA Aerospace Sciences Meeting, AIAA Paper 2009-0051, Orlando, FL, Jan. 2009.

[9] Gur, O., Bhatia, M., Mason, W. H., Schetz, J. A., Kapania, R. K., and Nam, T., "Development of Framework for Truss-Braced Wing Conceptual MDO," 6th AIAA Multidisciplinary Design Optimization Specialist Conference, AIAA Paper 2010-2754, Orlando, FL, April 2010.

[10] Green, J. E., "Laminar Flow Control—Back to the Future?," 38th Fluid Dynamics Conference and Exhibit, AIAA Paper 2008-3738, Seattle, WA, 23–26 June 2008.

[11] Jensen, S. C., Rettie, I. H., and Barber, E. A., "Role of Figure of Merit in Design Optimization and Technology Assessment," *Journal of Aircraft*, Vol. 18, No. 2, 1981, pp. 76–81. doi:10.2514/3.57468

[12] Malone, B., and Mason, W. H., "Aircraft Concept Optimization Using Parametric Multiobjective Figure of Merit," *Journal of Aircraft*, Vol. 33, No. 2, 1996, pp. 444–445. doi:10.2514/3.46960

[13] *DOT—Design Optimization Tools, Version 5.0, Users Manual*, Vanderplaats Research & Development, Colorado Springs, CO, Jan. 1999.

[14] Audet, C., Dennis, J. E., Jr., Moore, D. W., Booker, A., and Frank, P. D., "A Surrogate-Model-Based Method for Constrained Optimization," 8th AIAA/USAF/NASA/ISSMO Symposium on Multidisciplinary Analysis and Optimization, AIAA Paper 2000-4891, Long Beach, CA, Sept. 2000.

[15] *Metallic Materials and Elements for Aerospace Vehicle Structures*," U.S. Dept. of Defense, MIL-HDBK-5J, Jan. 2003.

[16] Pratt, K. G., and Walker, W. G., "A Revised Gust-Load Formula and Re-Evaluation of V-G Data Taken on Civil Transport Airplanes from 1933–1950," NACA Rept. 1206, 1955.

[17] Renzelmann, M. E., "Self-Monitoring Latch Pin Lock for Folding Wing Aircraft," The Boeing Co., U.S. Patent 5201479, April 1993.

[18] McCullers, L. A., "Aircraft Configuration Optimization Including Optimized Flight Profiles," *Proceedings of a Symposium on Recent Experiences in Multidisciplinary Analysis and Optimization*, J. Sobieski (ed.), NASA CP-2327, April 1984.

[19] Gur, O., Mason, W. H., and Schetz, J. A., "Full Configuration Drag Prediction," 27th AIAA Applied Aerodynamics Conference, AIAA Paper 2009-4109, San Antonio, TX, June 2009.

[20] Blackwell, J., "Numerical Method to Calculate the Induced Drag or Optimal Span Loading for Arbitrary Nonplanar Aircraft," NASA SP-405, May 1976.

[21] Grasmeyer, J., "A Discrete Vortex Method for Calculating the Minimum Induced Drag and Optimum Load Distribution for Aircraft Configurations with Noncoplanar Surfaces," Virginia Polytechnic Inst. and State Univ., Multidisciplinary Analysis and Design Center for Advanced Vehicles, Dept. of Aerospace and Ocean Engineering, Rept. VPI-AOE-242, Jan. 1997.

[22] White, F. M., *Viscous Fluid Flow*, McGraw–Hill, New York, 1974.

[23] Hopkins, E. J., and Inoye, M., "An Evaluation of Theories for Predicting Turbulent Skin Friction and Heat Transfer on Flat Plates at Supersonic and Hypersonic Mach Numbers," *AIAA Journal*, Vol. 9, No. 6, June 1971, pp. 993–1003. doi:10.2514/3.6323

[24] Hopkins, E. J., "Charts for Predicting Turbulent Skin Friction from the van Driest Method (II)," NASA TN D-6945, Oct. 1972.

[25] Cebeci, T., and Bradshaw, P., *Momentum Transfer in Boundary Layers*, McGraw–Hill, New York, 1977.

[26] Braslow, A. L., Bartlett, D. W., Wagner, R. D., and Collier, F. S., Jr., "Applied Aspects of Laminar-Flow Technology," *Viscous Drag Reduction in Turbulent Boundary Layers*, edited by D. M. Bushnell, and J. N. Hefner, Vol. 123, Progress in Aeronautics and Astronautics, AIAA, New York, 1990.

[27] Boltz, F. W., Kenyon, G. C., and Allen, C. Q., "Effects of Sweep Angle on the Boundary-Layer Stability Characteristics of an Untapered Wing At Low Speeds," NASA TN D-338, Oct. 1960.

[28] Wagner, R. D., Bartlett, D. W., and Collier, F. S., Jr., "Laminar Flow—The Past, Present, and Prospects," 2nd AIAA Shear Flow Conference, AIAA Paper 1989-0989, Tempe, AZ, March 1989.

[29] Romans, T., and Hirt, G., "Rolling of Drag Reducing Riblet Surface," 51st AIAA/ASME/ASCE/AHS/ASC Structures, Structural Dynamics, and Materials Conference, AIAA Paper 2010-3062, Orlando, FL, April 2010.

[30] Hoerner, S. F., *Fluid Dynamic Drag*, Hoerner Fluid Dynamics, Bakersfield, CA, 1965.

[31] Torenbeek, E., *Synthesis of Subsonic Airplane Design*, Delft Univ. Press and Martinus Nijhoff, Hague, The Netherlands, 1982.

[32] Jobe, C. E., "Prediction and Verification of Aerodynamic Drag, Part I: Prediction," *Thrust and Drag: Its Prediction and Verification*, edited by C. E. Eugene, Vol. 98, Progress in Astronautics and Aeronautics, AIAA, New York, 1985, Chap. 4.

[33] Shevell, R. S., *Fundamentals of Flight*, Prentice–Hall, Upper Saddle River, NJ, 1989.

[34] Nicolai, M. L., *Fundamentals of Aircraft Design*, METS, San Jose, CA, 1984.

[35] Raymer, D. P., *Aircraft Design: A Conceptual Approach*, 4th ed., AIAA Education Series, Reston ,VA, 2006.

[36] Mason, W. H., "Analytic Models for Technology Integration in Aircraft Design," AHS, and ASEE, Aircraft Design, Systems and Operations Conference, AIAA Paper 1990-3262, Dayton, OH, Sept.

[37] Inger, G. R., "Application of Oswatitsch's Theorem to Supercritical Airfoil Drag Calculation," *Journal of Aircraft*, Vol. 30, No. 3, May–June 1993, pp. 415–416. doi:10.2514/3.46354

[38] Hilton, H. W., *High speed Aerodynamics*, Longmans, Green and Co., London, 1951.

[39] Malone, B., and Mason, W. H., "Multidisciplinary Optimization in Aircraft Design Using Analytic Technology Models," *Journal of Aircraft*, Vol. 32, No. 2, March–April 1995, pp. 431–438. doi:10.2514/3.46734

[40] Tétrault, P.-A., Schetz, J. A., and Grossman, B., "Numerical Prediction of the Interference Drag of Strut-Surface Intersecting in Transonic Flow," *AIAA Journal*, Vol. 39, No. 5, May 2001, pp. 857–864. doi:10.2514/2.1389

[41] Hurel, M., "The Advantages of High Aspect Ratios," *Interavia, Aerospace World: Business and Technology*, Vol. 7, No. 12, 1952, pp. 695–699.

[42] Hallissy, J. B., and Phillips, P. S., "Wind-Tunnel Investigation of Aerodynamic Characteristics and Wing Pressure Distributions of an Airplane with Variable-Sweep Wings Modified for Laminar Flow," NASA TM-4124, 1989.

[43] Eggleston, B., Poole, R. J. D., Jones, D. J., and Khalid, M., "Thick Supercritical Airfoils with Low Drag and Natural Laminar Flow," *Journal of Aircraft*, Vol. 24, No. 6, June 1987, pp. 405–411. doi:10.2514/3.45460

[44] Kroo, I., "Nonplanar Wing Concepts for Increased Aircraft Efficiency," *Innovative Configurations and Advanced Concepts for Future Civil Aircraft*, VKI Lecture Series, von Karman Inst. for Fluid Dynamics, Rhode-Saint-Genèse, Belgium, June 2005.